POLITECNICO DI TORINO

MASTER OF SCIENCE IN PETROLEUM ENGINEERING

‹‹ Fluid-flow and geochemical simulations of CO_2 storage in a depleted gas reservoir: identification of the key parameters››

KOURLIANSKI ILIAS

Supervisor: Professor Verga Francesca

Torino, March, 2022

ACKNOWLEDGEMENTS

I would first like to express my sincerest gratitude to my professor, supervisor, mentor, Verga Francesca, for her continuous support, guidance, valuable advice, excellent cooperation, and intellectually stimulating conversations during the elaboration of my thesis.

I would also like to thank my dearest family who supported me throughout my studies with their help, love, encouragement, and support on all fronts.

I also warmly thank the professors of the Master's program for their selfless contribution, for the important time they devoted to me and for the valuable information they passed on to me throughout this two-year period.

I am grateful for the technical support, and the courses Computer Modelling Group provided on GEM and the supporting software.

Finally, I would like to thank all those dear friends and relatives who in their own special way supported, and motivated me for the completion of this work.

ABSTRACT

Carbon capture and storage (CCS) is one of the methods for the reduction of anthropogenic CO_2 emissions. Deep saline aquifers, and depleted oil and gas fields are all potential storage sites but they differ substantially for the quantity of CO_2 they can accommodate, and for the knowledge level and uncertainties characterizing them. Typically, depleted fields have a relatively limited capacity but they have been thoroughly investigated and information about their geological structure and rock properties are already available before conversion into a storage facility. Deep aquifers are potentially able to host very large CO_2 quantities but they are mostly unexplored traps and require significant investments to assess their suitability as safe CO_2 storage sites. This is the main reason why depleted fields are considered a very interesting option for CO_2 storage.

Along this line, this research was aimed at investigating the significance of modelling and quantifying the physical and chemical CO_2 trapping mechanisms taking place in a depleted gas reservoir where CO_2 is injected for geological storage.

The study was carried out with the aid of a commercial software specifically developed to model the CO_2 flow and the geochemical reactions in underground formations. The software is GEM, offered by the company Computer Modelling Group.

First, the simulation objectives were established, namely the investigation of the impact of each trapping mechanism of the stored CO_2 in a gas reservoir as a function of the rock – fluid interaction properties. A simplified reservoir geometry was assumed to avoid dependence of the results from a specific shape or layering of the geological formation. The data for characterizing the reservoir were mainly taken from the literature, based on published case histories describing in detail reservoirs successfully converted into CO_2 storages.

To have the most efficient storage, the pressure and temperature conditions were chosen so that CO_2 remains in the reservoir in the supercritical phase. After generating the reference model, two gas production scenarios were simulated to mimic the reservoir depletion. Then CO_2 was injected. The simulation time was much longer than the injection period so as to investigate the changes in the CO_2 distribution as a free fluid, as a trapped fluid, and as a mineral over time. The initial simulations only included structural trapping, then solubility trapping, capillary trapping, and mineral trapping were progressively added in the simulations to investigate the impact of each process on the CO_2 fate.

The results not only emphasized the importance of considering the geochemical trapping processes while designing and developing a CO_2 storage project but also highlighted which parameters have the largest impact on the modeled trapping mechanisms. This aspect is particularly relevant and of practical application when defining the laboratory experiments needed to characterize the system. Results confirmed

that the rock relative mineral volume fractions and the relative permeability curves are key information to be determined. Furthermore, it was found that water vaporization has a significant influence on the amount of mineral precipitate. Specifically, a large increase in the mineral precipitate was observed when water vaporization was modeled, which is a plus since mineral trapping is considered the safest trapping mechanism.

TABLE OF CONTENTS

CHAPTER 1

INTRODUCTION

1.1 Problem statement

While the international scientific and political community discusses climate change due to relative uncertainty, one preventative action is the decrease of global carbon dioxide emissions, since we have observed a 40% increase in the atmospheric concentration of CO_2 from 280 ppm in the pre-industrial era to 380 ppm today [1] (Figure 1) A rise in greenhouse gas emissions and a rise in atmospheric CO_2 concentrations are predicted as a result of increased global energy consumption and continued reliance on fossil fuels during this century [2]. Most of the greenhouse gas emissions come from burning fossil fuels, changing land use, and soil cultivation. According to estimates, power production accounts for 70 percent of the total CO_2 released into the atmosphere by combustion processes globally.

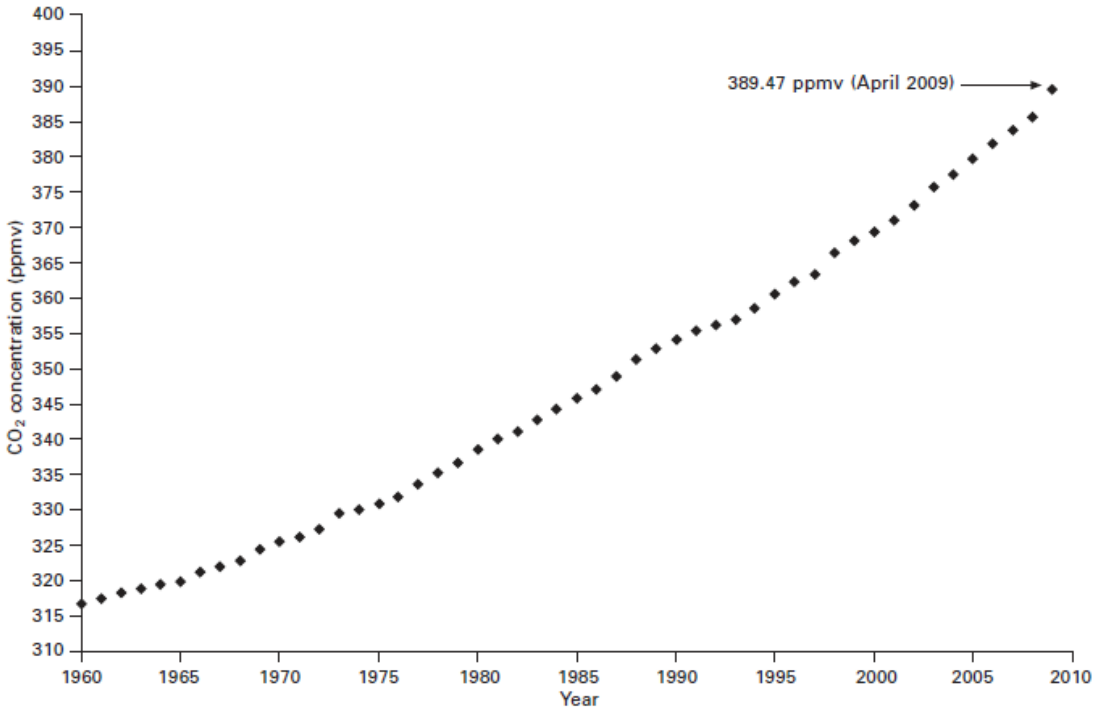

Fig. 1: Average annual atmospheric CO2 concentrations based on direct measurements at Mauna Loa Observatory from 1960–2009 (NOAA/ESRL) [62].

The 2015 Paris Agreement is aimed at limiting global warming to less than 2°C, preferably 1.5°C, by mid-century, compared to pre-industrial levels [3]. If the problem is

not addressed properly, we may experience an increase in temperature of 1.4 to 5.8 °C by the end of this century [4]. Also, 37 countries signed the Kyoto Protocol in 1997 as part of the United Nations Framework Convention on Climate Change in order to reduce greenhouse gas emissions. This treaty went into effect in 2005, and the number of countries that ratified it grew to 191 in 2011. With regard to CO_2 emissions, the goal was to reduce them over a five-year period (2008-2012) by a certain percentage, depending on where you live (8 percent in Europe and 7 percent in the USA) [5]. One mitigation strategy for stabilizing atmospheric greenhouse gases, as also addressed by the Intergovernmental Panel on Climate Change (IPCC) in 2005, is carbon capture and storage (CCS) [6].

CO_2 capture and storage is the process of capturing CO_2 from industrial sources, separating it from impurities like acidic gases or particulates, compress it for transportation, and finally inject it underground into sedimentary basins like deep saline aquifers, depleted oil and gas reservoirs or coal beds (Figure 2).

CCS must play a critical role in reducing CO_2 emissions to the atmosphere in order to limit further global warming and climate change until a low-carbon economy can be properly implemented if current living standards are to be maintained in the face of rising energy costs. Nevertheless, the world will almost certainly be dependent on coal and other fossil fuels until at least 2050. To make CCS more economically feasible on a large scale, additional research, innovation, and deployment are required. Many pilot-scale CCS projects are already operational, and many more are scheduled to begin in the near future.

Aquifers appear to be the most attractive sites for CO_2 storage because they are broadly distributed, underlie the majority of point sources of CO_2 emissions, and are not limited by reservoir size, as depleted oil and gas reservoirs are [7],[8]. However, in the case of oil and gas reservoirs, the same facilities can be used. Lastly, a smaller storage capacity at depletion makes oil reservoirs less attractive for long-term storage than gas reservoirs or aquifers. But they have the benefit of being best suited for CO_2 enhanced oil recovery (EOR), which increases their storage capacity while decreasing the cost of that storage by producing more oil. In this study, we concentrate on CO_2 storage in depleted gas reservoirs, and do not consider the usage of CO_2 for enhanced oil production in depleted oil reservoirs or storage in coal beds.

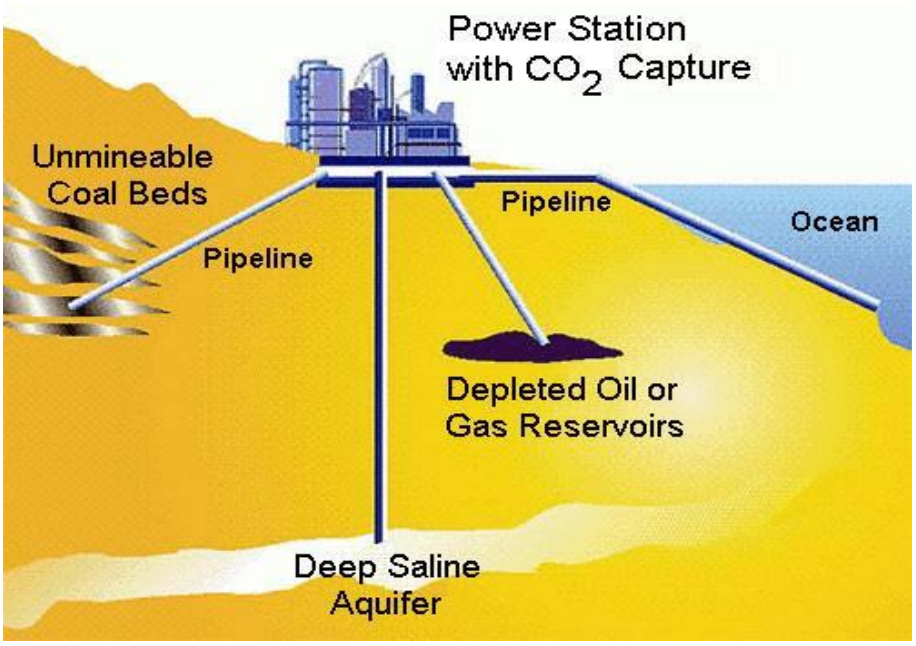

Fig. 2: Schematic of a carbon capture and storage [70].

The appeal of the CCS program also led governments and the private sector to make significant investments in developing the required technologies and trying to assess whether CO_2 monitoring could be implemented to maintain the CO_2 safely and effectively in reservoirs [9]. It was recognized early that geological storage could pose a threat to humans and local ecosystems in case of leakage through injection or abandoned wells, along fault lines, or inefficient confining layers. Because of this, cost-effective, reliable monitoring of the injected CO_2 must be an essential part of a storage project and made with respect to the unique features of every CCS. As a basic guideline, there are two sorts of monitoring: monitoring reservoirs to confirm their stability and integrity; and near-surface monitoring of water, air, and soil to guarantee public health and environmental protection. These two domains have different monitoring targets and equipment prerequisites, as stated in the IPCC and USDA (United States Department of Agriculture) reports [10-11]. As part of the Environmental Protection Agency's (EPA) authorizing processes for underground CO_2 injections, monitoring the fate of CO_2 has become compulsory [12-15]. Although, leaks in the range of 0.01 percent over the reservoir's expected lifespan are tolerable [10].

In addition, to develop the CCS technology on a big scale around the world we must ensure long-term CO_2 containment and storage security, which is primarily dependent trapping mechanisms. Characterization of dynamic storage behavior necessarily involves, among other things, an understanding of changes in formation fluid chemistry and subsequent reactions, as well as the application of reactive transport modelling to assess these processes. Batch models are also considered essential to identify key reactions, aqueous species, and minerals that are input parameters in the reactive transport models. Features like mineral composition and dissolution rates must be assessed to constrain conceptual models for long-term CO_2 trapping mechanisms, wellbore, and cap rock integrity. Injectivity has to be taken into account too, given that it plays a fundamental

role in making such projects possible. Low permeability formations, for example, naturally lead to low injection rates, which in turn will make the development questionable. Finally, with regard to safety, geomechanics, well completion and cementing, as well as geochemical issues, are crucial points to be considered as well.

1.2 Scope of work

The scope of this work is to investigate how to reliably predict and quantify the physical and chemical CO_2 trapping mechanisms that occur in depleted gas reservoirs where CO_2 is injected for geological storage. This was made possible by using a fully compositional EOS commercial simulator developed to model the geochemical reactions and supercritical CO_2 flow in the geological formation. The software suite was developed by the company Computer Modelling group, and it contains the simulator GEM, the pre-processor BUILDER, the post-processor RESUTLS, and the fluid characterization and phase behavior software WINPROP.

The simulation objectives were to determine the influence of the CO_2 trapping mechanisms in the reservoir as a function of the rock-fluid interactions. Then, a reservoir geometry was assumed, with data primarily derived from literature, based on reservoirs converted into CO_2 storages.

Gas production to simulate reservoir depletion and then CO_2 injection were first simulated. All the trapping mechanisms were taken into account: structural trapping, capillary trapping, solubility trapping, and mineral trapping. To explore changes in CO_2 distributions as a free fluid, trapped fluid, and mineral precipitate over time, the overall simulation time was substantially longer than the production - injection periods. CO_2 trapping processes was progressively added to the base model to investigate the impact of each process on the CO_2 fate.

CHAPTER 2

SITE SELECTION CRITERIA AND CHARACTERIZATION METHODS OF CCS

2.1 Introduction

The selection and characterization of the site is a crucial first step before any on-site development of a CCS project. The storage must prove that it can store the planned amount of CO_2 at the rate at which it is delivered without posing any inherent risk. As previously stated, it is anticipated that no leakage will occur at any selected site, or that if leakage occurs, it will be within appropriate limits over the reservoir's forecasted life. To identify, compare, and evaluate whether potential candidate sites meet the storage requirements, these sites must be ranked using a set of criteria. This chapter will address the framework for assessing prospective sites' appropriateness for CO_2 storage and ranking them for site selection, as well as methodologies for evaluating their storage capacity.

2.2 Assessment of site suitability

As of now, there is sufficient practical experience with the selection and characterization of sites for the injection of CO_2 around the world. Cook [16] gave one definition for site characterization, and described the process as: “the collection, analysis and interpretation of subsurface, surface and atmospheric data (geoscientific spatial, engineering, social, economic, environmental) and application of that knowledge to judge, with a degree of confidence, if an identified site will geologically store a specific amount of CO_2 for a defined period of time and meet all required health, safety, environmental and regulatory standards”. Several researchers have proposed so far various site screening and ranking frameworks. According to the research so far, site selection screening process comprises two parts. First screening takes place at the site and/or regional scale and the second, more in-depth screening takes place at the local and/or site-specific scale.

2.2.1 Site and regional scale screening

The table below (Table 1) shows the first set of elimination criteria that each region or site must meet in required to be deemed eligible for CO_2 storage. If a site fails to meet the first three criteria of the table, it is immediately considered unsuitable due to the risk of jeopardizing storage safety and security. On the contrary, with regard to the next four

essential criteria (4-7), there may be specific circumstances wherein a site may still be considered for CO_2 storage even if one of these criteria is not met but the rest are. Lastly, even though it is subject to change in the future, legal accessibility is crucial and eliminatory in and of itself.

	Criterion	Not Suitable	Suitable
1	Depth	Less than 1000m	Greater than 1000 m, with storage units deeper than 800 m
2	Reservoir seals and stratigraphic sequences	Poor	Intermediate and excellent. At least one major extensive, regional-scale competent seal
3	Pressure regime	Over-pressured	Hydrostatic or sub-hydrostatic
4	Seismicity	High and very high subduction zone	Very low to moderate
5	Faulting and fracturing intensity	Extensive	Limited to moderate
6	Surface areal extent	Less than 2500 km^2	Greater than 2500 km^2
7	Hydrogeology	Shallow, short flow systems, or compaction flow	Intermediate and regional-scale flow systems, topography and erosional flow
8	Legal accessibility	Forbidden	Possible

Table 1: Elimination criteria for evaluating regions and sites for CO_2 storage [16, 17, 18].

Besides the previous criteria, target reservoirs for injection are commonly sandy units with variable clay and silicate mineral composition that can be overlain by shale seals. Quartz sand and clays are characterized by low CO_2 reactivity, whilst carbonates, as well as plagioclase, feldspar and mafic minerals, have a higher reactivity [19]. In terms of grain size, larger grain sizes correspond to increased hydraulic conductivity at the cost of residual trapping efficiency [20]. Porosity and permeability are two more variables to consider when evaluating a formation. According to research, porosity in the 5-30% range

and permeability in the 200-3500 md range provide adequate reservoir volume and CO_2 injection rates [21, 22]. Pressure gradients dissipate gradually over time in low permeability rocks, and fluid pressure gradually rises near the injection well. Because of the need to avoid jeopardizing the overlying seal, the viable injection rate and accessible pore volume for a given well may be limited.

Other desirable CO_2 storage appropriateness criteria by which the site can be ranked and compared are listed in the following table (Table 2). None of these criteria are in and of themselves sufficient to rule out a site from consideration for CO_2 storage, and it is possible that a site may have several undesirable characteristics while still being considered for CO_2 storage. If, conversely, a site can be characterized by too many undesirable criteria, it should be considered whether to continue with the CCS. The first four criteria (1–4) correspond to the site's overall storage characteristics. The following five criteria (5–9) address the capability of storage in different geological formations. The last five criteria (10–14) are proxy measures for the economics of the storage.

	Criterion	Undesirable	Desirable
1	Withing fold belt	Yes	No
2	Significant diagenesis	Present	Absent
3	Geothermal regime	Warm basin (i.e., $> 40°C / km$)	Cold basins (i.e., $< 40°C / km$)
4	Evaporites (salt)	Absent	Domes and beds
5	Hydrocarbon potential	Absent or small	Medium to giant
6	Industry maturity	Immature	Mature
7	Coal seams	Absent, very shallow or very deep	At intermediate depth (400-800 m)
8	Coal rank	Lignite or anthracite	Sub-bituminous and/or bituminous
9	Coal value	Economic	Uneconomic
10	On/off shore	Deep offshore	Shallow offshore and/or onshore
11	Climate	Harsh	Moderate
12	Accessibility	Inaccessible/difficult	Good
13	Infrastructure	Absent or rudimentary	Developed

14	CO_2 sources within economic distance	Absent	Present

Table 2: Attractive characteristics of regions and sites eligible for CO_2 storage [16, 23, 24].

2.2.2 Site-specific and local scale screening

A site must not only meet the requirements for being deemed suitable for CO_2 storage and have attractive characteristics, but it must also pass additional site-specific screening criteria that apply only on a local scale. The elimination criteria can be split into the following three categories [16, 23, 24]:

- Lack of legal and/or physical access.
- Potentially affecting other resources whose production and/or utilization has primacy over CO_2 storage.
- Lacking security and safety.

When addressing these criteria, it must be taken into consideration that the storage is located at a depth in the subsurface but requires access from the surface.

1. Legally inaccessible (parks, military areas).
2. Legally unreachable (land access not permitted by authorities).
3. Legally unavailable (land or subsurface property owner that restricts access).
4. Physically unavailable (a reservoir still in production).
5. Located within high density population areas.
6. Potentially affecting other natural, energy and mineral resources and equity.
7. Within the depth of protected groundwater.
8. Located at shallow depth (800m is the minimum depth to maximize storage efficacy).
9. Lacking at least one major, extensive, competent barrier to upward CO_2 migration.
10. Located in an area of very high seismicity.
11. Located in overpressured strata.
12. Lacking monitoring potential.

Furthermore, there are additional desirable characteristics in this case that would make one site preferable to another. Failure to possess one of them, on the other hand, will not exclude it from consideration as a potential CO_2 storage site but will only reduce its desirability.

1. Sufficient capacity and injectivity.
2. Sufficient thickness (a minimum of thickness of 20 m is recommended to have variability in the injection strategies).
3. Low temperature (that in turn increases storage capacity and in generally storage security).
4. Favorable hydrodynamic regime (aquifers with regional scale flow systems are preferred).
5. Low number of well penetrating the storage of influence (possibility of leakage increases with the number of wells).
6. Presence of a multilayered overlying system of aquifers/reservoirs and aquitards/caprock (overall increase in the security in the sense of secondary containment).
7. Potential for attenuation of leaked CO_2 near and at surface (sites where CO_2 tends to accumulate are less desirable).
8. Site accessibility and infrastructure.
9. Storage economics.

2.3 Storage capacity estimation

The total area of the planet's sedimentary basins, excluding those located offshore, is nearly 70–80 million square kilometers [25]. Table 3 features the estimated storage capacities for the common geological formations considered for CCS.

	Sequestration option	Worldwide capacity (Gt CO_2)
1	Saline aquifers	100 - 10.000
2	Depleted oil reservoirs	120
3	Depleted natural gas	700
4	Deep coal seems	140

5	Deep saline basalt formations	>240
6	Organic shales	unknown

Table 3: Storage capacity estimations for the common geological formations [26].

In the oil and gas industry, both static and dynamic methods are used to evaluate subsurface hydrocarbon volumes. Static methods are a function of the volumes and compressibility of the fluids. Dynamic methods, on the other hand, involve curve analysis, material balance, and reservoir simulations, and they can only be applied after injection has commenced. As a result, only static methods will be summarized here based on Bachu's et al. work [24].

2.3.1 Gas reservoir capacity estimation

If the original gas in place (*OGIP*) is given at surface conditions, then the theoretical mass storage capacity for CO_2 storage in a reservoir at in-situ conditions (M_{CO2t}) can be calculated by:

$$M_{CO_2 t} = \rho_{CO_2 r} \times R_f \times (1 - F_{IG}) \times OGIP \times [(P_s \times Z_r \times T_r) / (P_r \times Z_s \times T_s)] \quad (1)$$

where, $\rho_{co_2 r}$ is the CO_2 density at reservoir conditions, R_f is the recovery factor, *Z* is the compressibility factor, F_{IG} is the fraction of the injected gas, and the subscripts 's', 'r' indicating surface or reservoir conditions respectively.

Alternatively, an equation based on the geometry of the reservoir may be used:

$$M_{CO_2 t} = \rho_{CO_2 r} \times [R_f \times A \times h \times \phi \times (1 - S_w) - V_{iw} + V_{pw}] \quad (2)$$

where, *A, h,* ϕ, and S_w are the reservoir's area, thickness, porosity and water saturation respectively. V_{iw} and V_{pw} are the volumes of the injected and produced water respectively.

If the reservoir has an underlying aquifer, three factors influence the effectiveness of the CO_2 storage process.

- CO_2 mobility with respect to the other fluids.
- CO_2 density contrast that leads to segregation.
- Reservoir heterogeneity.

These factors reduce the available volume for storage and are expressed in the form of capacity coefficients ($C<1$). In addition, they are used in the calculation of the effective reservoir capacity (M_{CO2e}):

$$M_{CO_2e} = C_m \times C_b \times C_h \times C_w \times C_a \times M_{CO_2t} = E \times M_{CO_2t} \quad (3)$$

where the subscripts 'm', 'b', 'h', 'w' and 'a' stand for mobility, buoyancy, heterogeneity, water saturation and aquifer strength respectively. E is the storage efficiency coefficient.

2.3.2 Saline aquifers capacity estimation

The process of CO_2 storage in aquifers is comparable as in depleted gas reservoirs. If the geometric volume of the structural or stratigraphic (V_{trap}) along with its porosity and irreducible water saturation (S_{wirr}), are known, therefore the theoretical volume available for CO_2 storage (V_{CO2t}) can be determined using the following equation:

$$V_{CO_2t} = V_{trap} \times \phi \times (1 - S_{wirr}) = A \times h \times \phi \times (1 - S_{wirr}) \quad (4)$$

where, A and h are the trap's area and average thickness respectively. Since in equation (4) porosity and irreducible water saturation are considered constant, this equation should be applied when average values used.

As result, the effective storage volume (V_{CO2e}) is calculated by:

$$V_{CO_2e} = E \times V_{CO_2t} \quad (5)$$

where E is the storage efficiency coefficient as in the gas reservoirs' calculations.

Moreover, in order to calculate the respective CO_2 mass, the CO_2 density inside the trap must be known which is dependent on the pressure of trap filled with CO_2. Despite the fact that the trap volume is constant, the CO_2 stored mass can fluctuate due to pressure variations, which affect CO_2 density. To achieve injection in the first place, however, the pressure must be greater than the initial pressure in the trap. Simultaneously, it must be less than the maximum allowable bottom hole injection pressure to avoid rock fracturing but also capillary seal breaching. So, we can write the following relationship for the (M_{CO2e}) [78].

$$\begin{aligned} \min M_{CO_2e} &= \rho_{CO_2}(P_i, T) \times V_{CO_2e} \le M_{CO_2e} \\ \max M_{CO_2e} &= \rho_{CO_2}(P_{\max}, T) \times V_{CO_2e} \ge M_{CO_2e} \end{aligned} \quad (5)$$

One suggestion of the US Department of Energy is to estimate the volumetric CO_2 storage capacity by using the entire volume of the aquifer according to the following relationship [27]:

$$M_{CO_2e} = \rho_{CO_2} \times E \times A \times h \times \phi \quad (6)$$

where ρ_{co_2} is the average CO_2 density at the estimated reservoir conditions for a specific aquifer. The influence of irreducible water saturation is not distinctly considered in the previous equation, but it is incorporated into the efficiency factor E via the pore scale displacement efficiency.

In case the aquifer is of great areal extent and features variabilities, an integral form of the equation 6 is advised.

$$M_{CO_2e} = E \times \iint \phi \times \rho_{CO_2} \times dAdh \quad (7)$$

CHAPTER 3

LITERATURE REVIEW ON GEOLOGICAL CO_2 SEQUESTRATION

3.1 Introduction

This chapter reviews the site characterization methods and the selection criteria of a CO_2 storage, as well as the physical and chemical mechanisms for underground CO_2 sequestration in deep geological formations.

3.2 Carbon capture and storage in geological formations

The first proposal of storing CO_2 in geological formations was made in the '70s. However, research into this field commenced in the '90s. Since then, important advances have been achieved in the available technologies to predict the future of injected CO_2. That has allowed to produce a broad range of work in several aquifers and to determine the feasibility of such a project. In Sleipner's gas field in the Norwegian North Sea, the first successful CO_2 sequestration test was conducted on a brine-bearing formation [28]. During this project, CO_2 was cleared out of natural gas which was then injected into the Utsira sand formation. The operations started in 1996 with an injection rate of 1 MMTPA. More than 15 MMTPA of CO_2 have been injected up to now without any significant problems encountered [29],[30]. Since then, other similar projects have been planned and developed all around the world, but still significant uncertainties exist.

The International Energy Agency (IEA) Greenhouse Research and Development program says that hydrocarbon reservoirs' storage capacity is approximately 920 Gt, whereas deep saline aquifers can store between 400 and 11.000 Gt. Compared to the 25 Gt worldwide CO_2 emissions per year [31].

The geological formations which are selected in CCS projects are in general permeable and have high temperature and pressure. This is due to the fact that CO_2 is normally injected as a supercritical fluid. The critical point being at 31,1 °C, and 73,8 bar (Figure 3). Above the critical point, pure CO_2 exists as a supercritical dense phase, with gas-like viscosity and liquid-like density much higher than that at atmospheric conditions (Figure 4). Whereas, below the critical point, it can exist as gas or liquid.

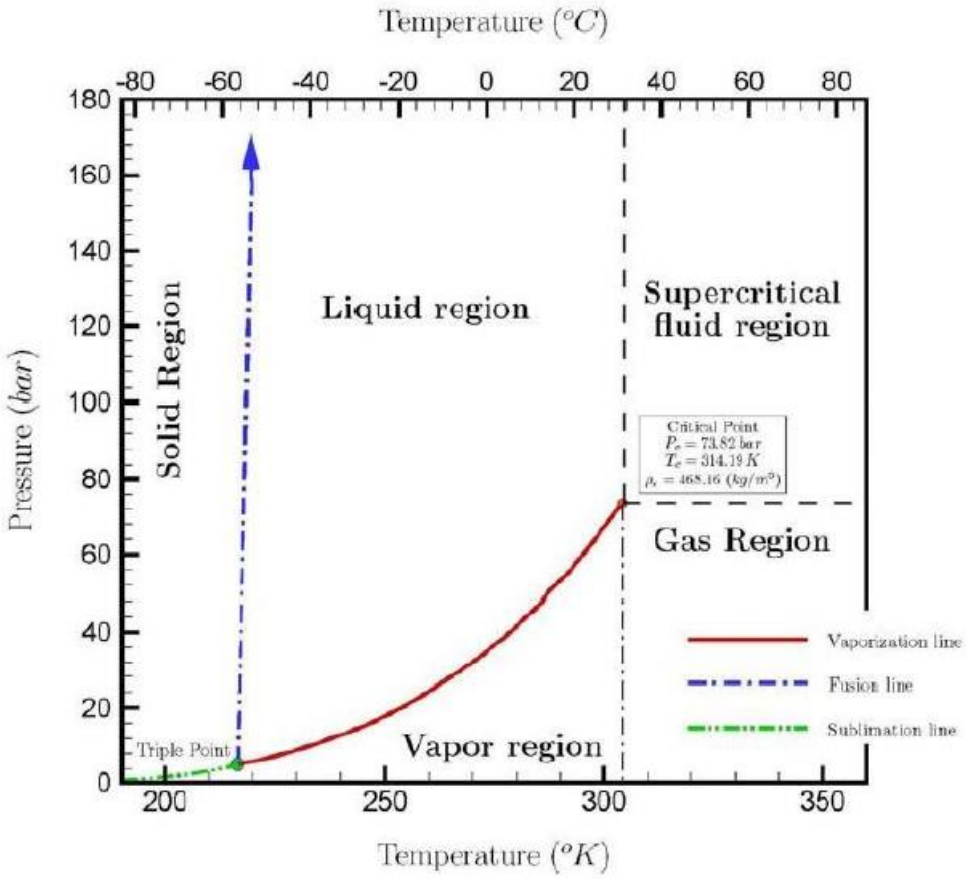

Fig. 3: CO_2 phase diagram (1 bar = 0,1 MPa) [32].

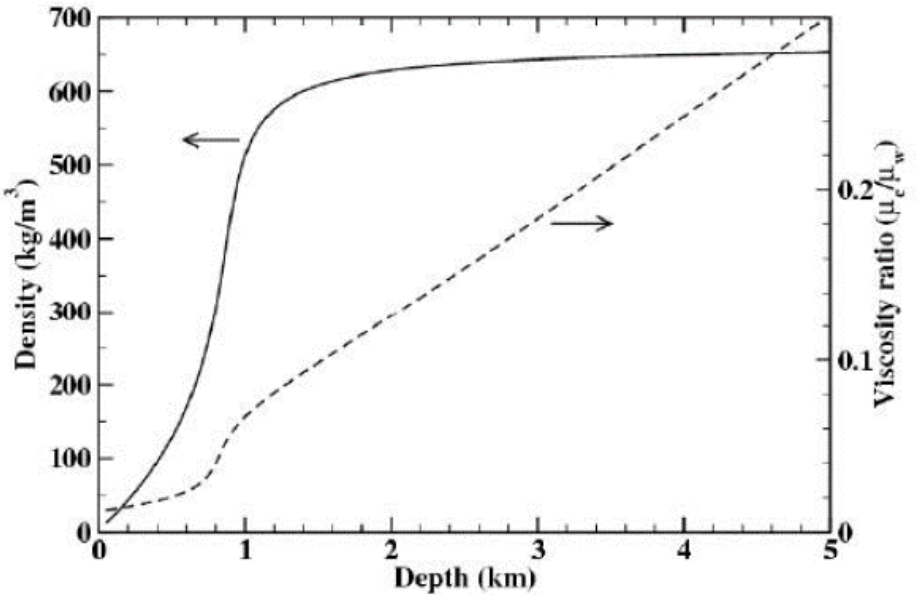

Fig. 4: CO_2 viscosity and density at subsurface conditions. Temperature and pressure gradients are 30 °C/km and 100 bar/km respectively [33].

By combining the ranges of surface temperatures (15-20°C), geothermal gradients (25-35°C/km) and, hydrostatic pressure gradients (105-160 bar/km), a range of potential injection conditions above atmospheric conditions can be derived (Figure 5). Between this range, a dense immiscible CO_2-rich fluid and an H_2O-rich liquid phase coexist.

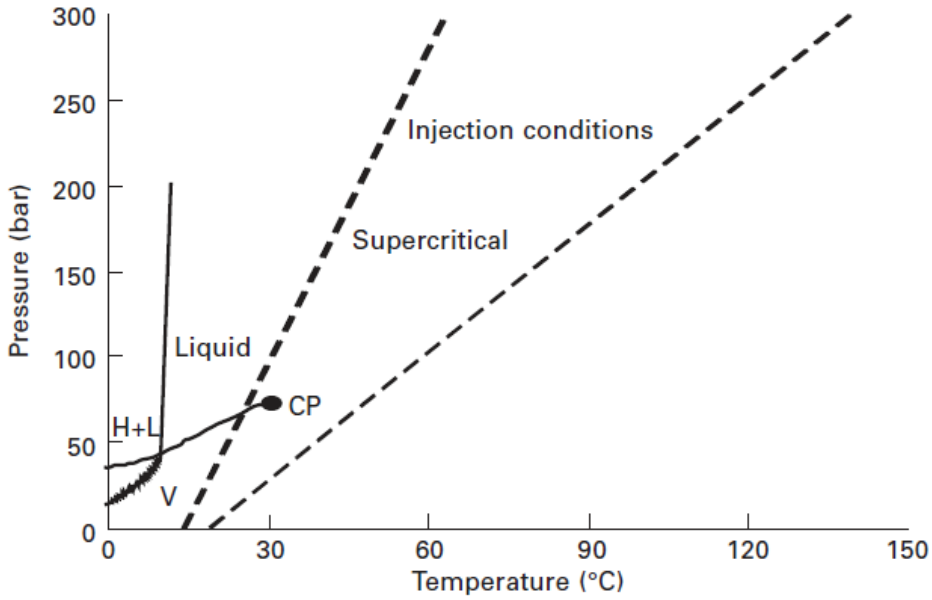

Fig. 5: Range of potential injection conditions above atmospheric conditions and up to 150 °C and 300 bar. Projections are extrapolated to surface conditions. CP is the CO_2 critical point. H, L, V stand for hydrate, liquid, and vapor respectively [34].

In aquifers CO_2 will tend to move upwards in the injected formation due to the density contrast with the formation fluids and because of buoyancy forces. Since the long-term interest in CO_2 trapping is centuries to thousands of years, it's essential that the selected structure avoids any gas escape. In addition to a cap-rock which serves as a seal, CO_2 is also trapped because of the interactions with the formation which control its migration and distribution throughout the subsurface. These processes include various chemical reactions, mineral dissolution and capillary trapping [35]. Consequently, they should be considered in the design of CO_2 storage projects.

3.3 Simulation of CO_2 trapping

In order to make sure the CO_2 is retained in the formation after its injection, it is essential that we monitor its subsurface activity. This is achieved through:

- Reservoir simulation, where the CO_2 distribution in the system is predicted during and after injection, so that efficient decision can be made [35].
- Geophysical measurements, for instance, seismic, electrical, and gravity, provide mapping of CO_2 saturation across the field.

Flow simulation is considered a necessary step in designing a CO_2 sequestration project, which in turn facilitates the creation of an injection strategy that increases the reservoir's storage volume while mitigating the chance of gas leakage. Specific data on physical and chemical processes during the sequestration process is, nevertheless, needed in order to obtain a representative simulation of the project [36].

3.3.1 Geochemical processes

The physical and chemical processes that have to be taken into account during flow simulation are:

- Gravity segregation.
- Residual CO_2 trapping (capillary trapping).
- Dissolution.
- Chemical processes (ionic trapping).

3.3.1.1 Gravity segregation

In aquifers, due to the density and viscosity of CO_2 being lower than that of formation water, CO_2 migrates upwards in the formation under buoyancy forces, finally reaching the top seal. This phenomenon is called gravity segregation and is illustrated in figure 6 [37]. While a gravity displacement between gas and oil is demonstrated in this figure, a similar process between gas and water is expected as both oil and water have a greater density than gas.

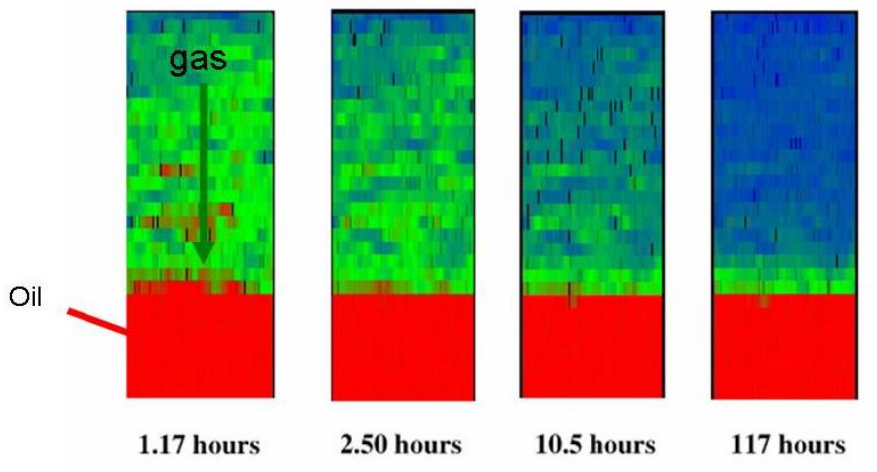

Fig .6: Gravity segregation phenomenon. The gas moves in from the top, as the density contrast between the phases makes the pressure difference greater than the capillary pressure. This lasts until gas and oil are in gravity equilibrium [38].

3.3.1.2 Residual CO_2 trapping (capillary trapping)

The simultaneous two-phase flow of CO_2 trapping occurs in porous media and plays an essential part in the migration and distribution of CO_2. It is also the process that takes place more quickly than the other processes of sequestration [39]. Snap-off is the dominant water-wet media trapping mechanism undergoing a capillary flow regime [39]. When water fills narrow areas of pores, snap-offs are observed leaving droplets of CO_2 surrounded by water.

The reservoir's gas saturation increases as the gas phase advances upwards because of buoyancy forces during the injection of CO_2. This migration continues after injection gas gets trapped on the forefront of the CO_2 plume as it rises during a drainage process. Conversely, water will displace the gas in an imbibition process at the rear end, which will ultimately snap off and induce gas trapping. In the end, this leaves behind a trail of immobile CO_2, which lies behind the migrating plume and is trapped as droplets surrounded by water (Figure 7) [40],[41]. Consequently, a model that captures relative permeability hysteresis is required for the macroscopic modelling of this process [42].

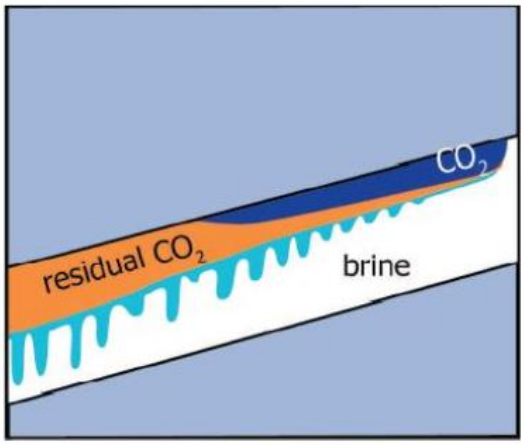

Fig. 7: Schematic of the trail left by the snap-off of residual CO2 while the plume moves upwards [39].

3.3.1.3 Dissolution

As a result of CO_2 solubility, part of the CO_2 injected is dissolved in the formation water. The quantity of CO_2 that dissolves in water changes depending on the aqueous phase pressure, temperature, and salinity. This process takes place when the phases come into contact, by mass transfer from the CO_2 to the aqueous phase [43]. Furthermore, water also has a certain solubility in CO_2, which can lead to dried-out brine and so, salt precipitation is observed [44], [45]. Three mechanisms govern the dissolution of CO_2 in formation water:

- CO_2 diffusion in the aqueous phase, which allows further CO_2 dissolution in the aqueous phase from the gas phase.

- Chemical interactions between the host rock and the dissolved CO_2.
- Effect of convective mixing, is considered as the prevalent CO_2 dissolution mechanism since it is much quicker than the rest and significantly improves CO_2 dissolution. This occurs when the CO_2-saturated water density is around 1% higher than unsaturated one [46].

3.3.1.4 Chemical processes (ionic trapping)

CO_2 dissolution in water produces a weak acid (1) that can then lead to the precipitation of carbonates by reacting with the rock. For instance, calcite dissolution can be represented by the relationship (2). This phenomenon is called mineral trapping and leads to the immobilization of CO_2 [33]. This effect, however, depends on the type of rock, the composition of the minerals constituting the rock, temperature, pressure, and porosity. In addition, laboratory experiments and numerical simulations reveal that these reactions induce changes in permeability and porosity which are transient and spatially dependent [47].

$$H_2CO_3 = H^+ + HCO_3^- \quad (1)$$

$$CaCO_3 + CO_2 + H_2O \rightarrow Ca^{2+} + 2HCO_3^- \quad (2)$$

3.3.2 Trapping mechanisms

To ensure the long-term CO_2 containment and the security of the storage, four trapping mechanisms have been proposed:

- Structural and stratigraphic trapping.
- Mineral trapping.
- Solubility trapping.
- Residual CO_2 trapping (capillary trapping).

Their contribution to CO_2 trapping as a function of time can be seen in the next figure (Figure 8).

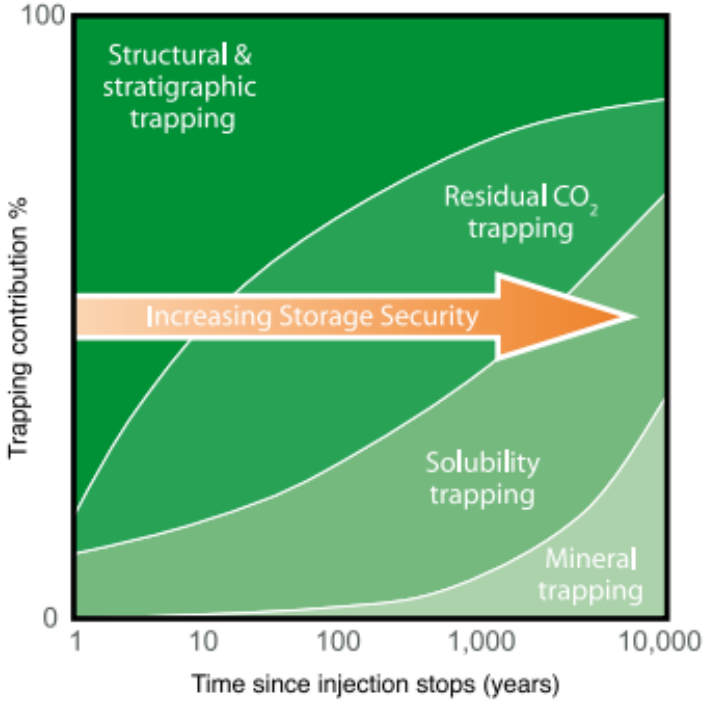

Fig. 8: CO_2 trapping contribution of the four mechanisms as a function of time [4].

Long-term containment measures fall into three categories: CO_2 trapping, well integrity, and caprock integrity (Figure 9).

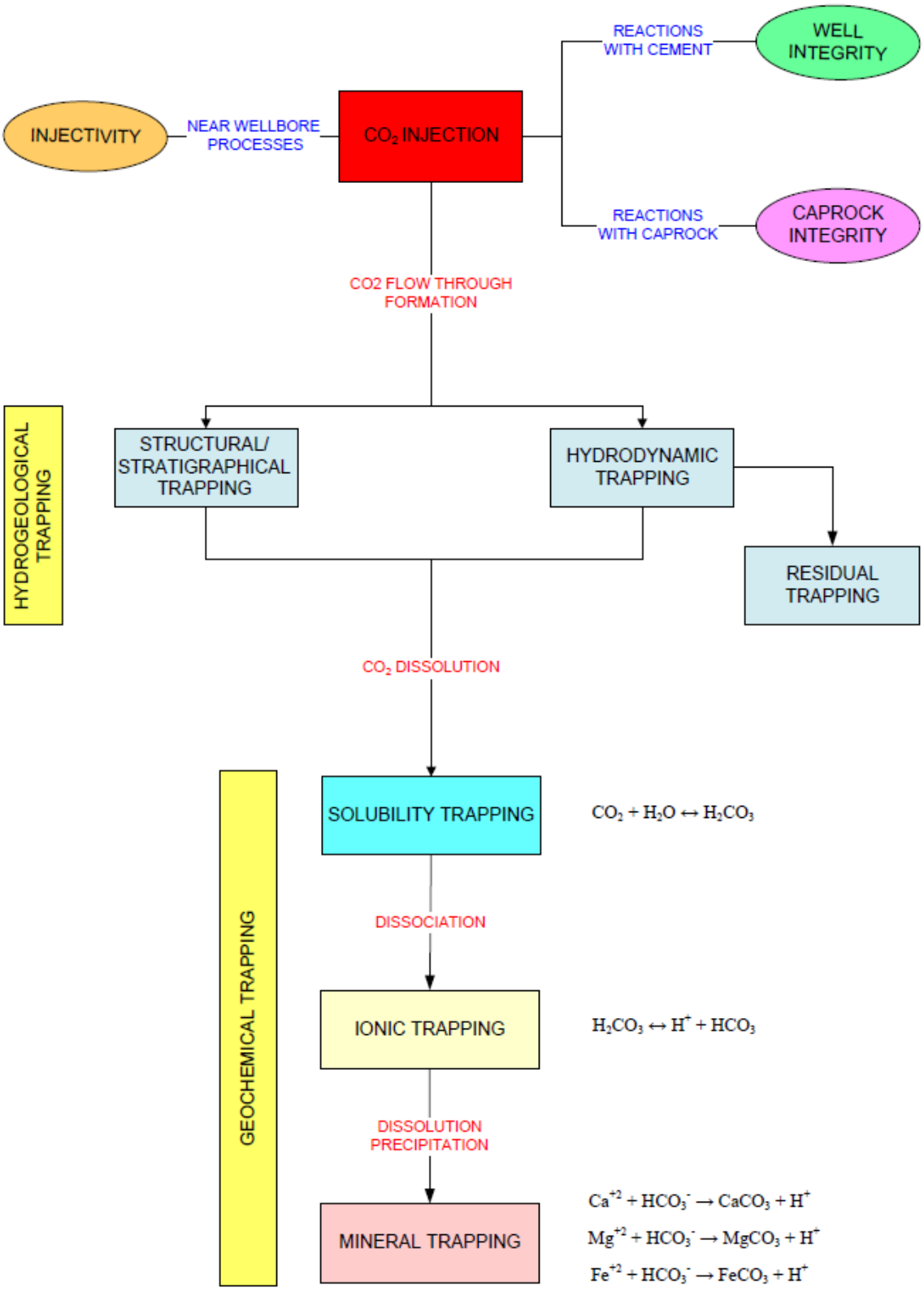

Fig. 9: Geochemical CO_2 processes in CCS [56].

3.3.2.1 Structural and stratigraphic trapping

As can be observed from the above figure, structural and stratigraphic trapping plays a vital role in CO_2 containment, especially during the first 10 years of the project and, is the only mechanism that is unlikely to change, since we rely on the geological structure. This mechanism relies on an impermeable bed at the top of the formation that serves as a seal. It is nevertheless necessary, to guarantee that the seal will not leak through passageways or by wells that penetrated the formation, through which the CO_2 could escape to the surface [48].

3.3.2.2 Mineral trapping

In this process, CO_2 chemically reacts with the rock and becomes part of the solid. While this is considered the safest mechanism, it is also the least important of the four as it takes millions of years to develop. For instance, precipitation of calcite can be represented by relationship (3).

$$Ca^{2+} + HCO_3^- \rightarrow CaCO_3 + H^+ \quad (3)$$

3.3.2.3 Solubility trapping

Injected CO_2 will progressively dissolve into the formation brine, leading to an increase in its density, and as a consequence, the mixture will sink gradually and will not reach the surface. This mechanism is solubility trapping.

$$CO_2 + H_2O = H_2CO_3 \quad (4)$$

3.3.2.4 Residual CO_2 trapping (capillary trapping)

When CO_2 is injected into an aquifer it displaces the brine and moves upwards under buoyancy forces. Reaching the top and flowing as a single phase, the front of the CO_2 plume displaces water in a drainage process, whereas at the tail the water displaces CO_2 in an imbibition process [49]. Water being the wetting phase, during the imbibition process, the films of water thicken and snaps off the pore throats, leading to trapping of bubbles of gas in the pores as a residual phase.

	Mechanisms	Duration after injection
Physical	Static trapping: the flow of CO_2 is impeded by a physical low-permeability barrier.	Duration is up to dozens of years after injection.
	Residual CO_2 trapping: the CO_2 is trapped in the pore space at irreducible gas saturation.	Duration can be up to thousands of years.
	Hydrodynamic trapping: a combination of different mechanisms, including all the possible physicochemical mechanisms.	Primary trapping is up to dozens of years while secondary trapping is up to a geological scale after injection.
Chemical	Adsorption trapping: the CO_2 is adsorbed onto organic materials contained on coals and shales.	Duration is up to dozens of years after injection.
	Dissolution trapping (solubility and ionic trapping):	Duration is up to hundreds of years.
	Solubility: $CO_{2(gaseous)} \rightarrow CO_{2(aqueous)}$ and $CO_{2\ (aqueous)} + H_2O \rightarrow H_2CO_{3(aqueous)}$	
	Ionic: $H_2CO_{3(aqueous)} + OH^- \rightarrow HCO_{3\ (aqueous)}^- + H_2O$	
	Mineral trapping: chemical reactions with the rock matrix in rich of Ca and Mg minerals. $HCO_{3(aqueous)}^- + OH^- \rightarrow CO_{3(aqueous)}^- + H_2O$ and $CO_{3(aqueous)}^- + Ca^{2+} \rightarrow CaCO_{3(solid)}$	Duration is up to a geological scale (tens of thousands to millions of years).

Table 4: CO_2 sequestration mechanisms in geological formations [50].

3.3.3 Caprock integrity

To ensure that any leaks are avoided throughout the life of a CCS project, the long-term behavior of the injected CO_2 is necessary to be studied. During the early stages it is especially important to monitor the caprock's integrity as the hydrogeological trapping mechanisms are prevalent.

In aquifers, as CO_2 migrates upwards towards the caprock it can dissolve in the formation water and diffuse into the caprock due to the concentration gradient. In turn, this can lead to water acidification and may result in both dissolution and precipitation that either impair or enhance the integrity of the seal. If CO_2 saturated brine gets rich in

divalent cations as reservoir rock minerals dissolve, when the brine diffuses into the caprock, carbonates may precipitate because of the higher pH of caprock brine and the lower partial CO_2 pressure. Carbonate precipitation improves the caprock's sealing capacity. Conversely, the caprock's acidic water increases permeability and forms a migration path, which additionally increases the permeability and the leakage of the fluid [51, 52].

3.3.4 Well integrity

Conventional well completions use cement as a seal in-between the casing and the formation. CO_2, in presence of water, may cause severe corrosion to the infrastructure due to the formation of carbonic acid, as well as mineralogical alternation of the cement. Even though the design of well completion is for a few decades, their integrity becomes questionable for a longer period. As a result, preventing casing damage and modelling cement alternation is of paramount importance to avoid any risk of leakage through the well and to guarantee that CO_2 is contained on a long-term basis.

Cement is a highly alkaline mixture that contains hydrated silicate and calcium aluminosilicate. The main process which is responsible for deteriorating cement is carbonation [52]. Dissolved CO_2 reacts with the constituents of the cement, forming calcium carbonate and calcium bicarbonate migrating out of the cement, something that increases permeability and porosity [53]. On the contrary, CO_2 ganglia are highly solvent and are able to transport a wide range of components from the reservoir rock which may cause cement alteration.

3.3.5 Near wellbore processes and impact on injectivity

In order to understand how the displacement of CO_2 changes in the vicinity of the wellbore and to ensure adequate injectivity of the planned CO_2 volume in the course of the injection period, geochemical modelling of this zone is necessary step.

In the near wellbore zone, the flow rate varies affected by, chemical dissolution and precipitation processes, the rock formation, composition of fluids and the prevalent thermodynamic conditions. This is crucial, since dissolution depends on the injection rate and variations of the flow rate will lead to different dissolution patterns [53].

An additional phenomenon that occurs during injection is drying. Drying leads to a permeability decrease because of the vaporization of water which causes solid concentration in the formation brine, which eventually precipitate [54]. Sodium chloride, being abundant in formation brines, will be the first to deposit because of vaporization. Since the saturation front moves away from the well very quickly, only a small quantity of precipitate is able to deposit. That being said, the salt precipitation could be sufficiently high to block the pores if the formation brine salinity is high and, at the same time, the

capillary imbibition is strong [55]. Nevertheless, in case of doubts, a low salinity or freshwater brine pre-flush can be followed preceding the CO_2 injection.

CHAPTER 4

STATE OF THE ART IN GEOCHEMICHAL MODELLING

4.1 Introduction

The establishment of a theoretical framework is deemed a necessary step towards understanding the interactions between CO_2, brine, and rock in aquifers and reservoirs. The target is to use models to better understand and anticipate the geochemical changes that occur in the reservoirs as a result of the injection of CO_2. A model consists of a set of equations with variables that represent the system's key parameters and is based on the principles of mass conservation. Real systems are complicated, and models are simplified versions of these systems, yet they are nevertheless important tools for understanding and forecasting the systems' behavior [56].

Geochemical models are based on three key processes: thermodynamics, reaction kinetics, and process flow and transport. The two types of geochemical models are:

- Batch models, which are referred to as those which do not take into account the flow and transport processes.
- Models which combine geochemical, flow, and transport reactions are referred to as reactive transport models.

This chapter aims at giving an overall picture of the thermodynamic and kinetics modelling approaches during simulations with batch and reactive transport models, specify the parameters and type of data necessary in CO_2 storage applications, as well as their constraints.

4.2 Thermodynamic equilibrium in geochemical modelling

Thermodynamics indicates the direction and the reactions that will take place as the system reaches equilibrium. In the case of a real systems' equilibrium, the properties of a system do not change in an indefinite period. Thermodynamic equilibrium is the main assumption of geochemical speciation modelling. Speciation modelling aims at forecasting the distribution of species, their activities, redox state, fugacities of gases, and degree of saturation of brine.

However, to apply thermodynamics to natural systems, since these systems are ever-evolving, we cannot assume broad equilibrium in our models, instead there is the necessity to adopt local equilibrium. In the context of local equilibrium, we apply

thermodynamics to systems that are not far away from equilibrium. Furthermore, based on this assumption, the general reactions can be broken down into a number of steps, in which thermodynamic equilibrium is applied every time.

The equilibrium composition of the system is identified through two approaches:

- LMA or law of mass action, by which the species' mass is readjusted up to the point that equilibrium is achieved by using equilibrium constants as limits.
- GEM or Gibbs energy minimization, by which the total system's Gibbs energy is directly minimized based on limitations of material balance.

4.2.1 Equilibrium in aqueous solutions

From thermodynamics, we know that chemical equilibrium is achieved when the Gibbs free energy of reactants and products are equal. Gibbs law is given by the formula:

$$G = H - TS \tag{1}$$

where G is the free energy, H is the enthalpy, T is the temperature in Kelvin, and S is the entropy. The equation above can be written in such a way that expresses the standard Gibbs energy of a reaction as:

$$\Delta_r G^\circ = \Delta_r H^\circ - T\Delta_r S^\circ \tag{2}$$

where $\Delta_r G^\circ$ is the reaction's standard Gibbs free energy, $\Delta_r H^\circ$ is the reaction's standard heat, and $\Delta_r S^\circ$ is the reaction's standard entropy change, and Δ_r indicates products minus reactants. Since we cannot measure absolute values, but only differences in Gibbs free energy and enthalpy, the formation Gibbs free energy $\Delta_f G^\circ$ and formation enthalpy $\Delta_f H^\circ$ are measured for any substance.

When equilibrium is reached the total Gibbs free energy,

$$\Delta G = \Delta G^\circ + RT \ln Q = 0 \tag{3}$$

and the ionic activity can be called as thermodynamic equilibrium constant K ($Q = K$). Codes used in geochemical modelling solve the equilibrium state by equilibrium constants or Gibbs free energies as well as provide databases where $\log K$, $\Delta_f G^\circ$, and $\Delta_f H^\circ$ are given in tabular form.

4.2.2 Activity and activity models

In the case of geochemical modelling of carbon storage, in order to describe the non-ideality of the real solutions, we use the parameter of activity which equals the effective concentration of a species in a chemical reaction. Because the electrostatic forces of the ions are stronger in real solutions than in ideal ones, the Gibbs free energy of real solutions is lower. It's because of this that species' chemical potentials are lower as well. Ion activity is a function of pressure, temperature, and the composition of the solution. Additionally, it is lower than its concentration.

Using the equation of Nernst, the chemical potential for real solutions can be expressed as:

$$\mu_i = \mu_i^{\circ} + RT \ln(\alpha_i) \tag{4}$$

where μ_i° is the chemical potential at standard state, R is the universal gas constant and α_i is the activity of species *i*, which is connected to its molarity by:

$$\alpha_i = \gamma_i m_i$$

where γ_i is the activity coefficient of the species *i.* In ideal solutions, the activity coefficient is equal to unity. However, since real solutions are electrically balanced, the activity coefficients of individual ions cannot be determined. As a result, the activity coefficients of individual ions are expressed by the mean activity coefficient of neutral electrolytes which can be measured. The mean activity of neutral electrolytes can be expressed by the equation:

$$\log \gamma_{\pm} = \frac{v_M \log \gamma_M + v_X \log \gamma_X}{v_M + v_X} \tag{5}$$

where v_X is v_M are the number of moles of anions and cations formed by dissociation of one mole of electrolyte.

Individual activity coefficient values are separated in a conventional manner [56]. The two methods used in geochemical modelling to calculate activity coefficients are:

- Debye-Hückel methods.
- Pitzer methods.

Debye-Hückel methods are characterized by their simplicity since the extrapolation over the range of temperatures can be performed easily, as well as the addition of new species. In contrast to the Pitzer methods, they provide information about the distribution

of the species but are unreliable at high ionic strengths and in solutions where sodium chloride is not the dominant solute. Inversely, the Pitzer methods are more precise at high ionic strengths but to use them, a lot of parameters are necessary. In addition, the data available is limited, and the components of silica and aluminum are unknown. Lastly, it's not yet possible to estimate the interaction parameters for aqueous species or extrapolate over a wide range of temperatures and pressures [57].

4.2.3 Numerical implementation in geochemical models

In order to define the aqueous composition in a geochemical model, there are a number of fundamental species that describe all of the species present in solution. These components meet the following criteria:

- Capable of forming all phases and species that were taken into account in the geochemical model.
- Be the minimum number needed to satisfy the first rule.
- Be independent of one another.

For instance, when carbon dioxide dissolves in water, the aqueous composition can be described with respect to the components H_2O, H^+, CO_2(aq.). Afterwards, chemical reactions between the fundamental species are carried out in order to express the secondary species such as, $OH^-, H_2CO_3, HCO_3^-, CO_3^{2-}$ [56].

Finally, the governing equations that have to be solved using iterative methods are split in three categories:

- Charge balance equations.
- Mass action equations.
- Mass balance equations.

4.3 Kinetics modelling

When the time scale is long enough to allow the system to reach equilibrium, or the reactions take place at a very fast rate, a thermodynamic equilibrium approach is appropriate. However, thermodynamic equilibrium models do not provide any data on how much time is necessary to reach equilibrium, nor they provide any data on transition states. Regarding carbon storage, it is crucial to know how long it will take before equilibrium is reached in the reservoir after the injection of CO_2. It is therefore apparent that slow reactions like mineral dissolution and precipitation, require the addition of a time variable to model the reaction's progression with time. Implementing a kinetics-

based modelling approach, this can be accomplished. The kinetics approach is linked with the thermodynamic approach since when equilibrium is established, mineral dissolution and precipitations rates are equal.

4.4. Implementing reactive transport models in geochemical modelling

When CO_2 is continuously injected into a geological formation the equilibrium conditions of the system are constantly altered. The dependency of the progression of chemical reactions from flow and transport processes is not considered in the static systems mentioned earlier in the chapter. It is then necessary to couple the transport, flow, and chemical processes in a dynamic model, to accurately simulate the evolution of the geochemical reactions in both spatial and temporal domains. This is achieved with reactive transport models, and flow is discretized into a series of interconnected stirred tank reactors [56]. The governing equations of reactive transport models can be split into two categories, equations that describe the fluid flow, and equations that describe reaction and transport kinetics. To solve these, finite element or finite difference numerical methods are applied. Moreover, different approaches are utilized in reservoir simulators in order to couple flow, transport, and reaction processes, such as:

- Sequential iterative approach.
- Sequential non-iterative approach.
- One-step approach.

Nevertheless, despite the fact that reactive transport models are better suited for geochemical modelling of carbon storage, they still rely on batch models. To indicate the key reactions, aqueous species, and minerals to include in the reactive transport models, batch models are used.

4.5 Solubility models of CO_2 in aqueous solutions

Another critical aspect that has to be taken into consideration in geochemical codes, is the amount of CO_2 that dissolves in the formation brine. A model that accurately predicts the CO_2 solubility in brine is required, or the thermodynamic data must be adjusted. Incorporating this type of model allows for the accurate calculation of the aquifer's storage capacity, along with indications of the brine-rock interactions. CO_2 solubility in brine is a function of the temperature, pressure, and salinity of the reservoir. In particular, CO_2 solubility decreases with increasing temperature, increasing salinity, and decreasing pressure. Consequently, the model must be valid for the range of the values of these parameters.

Dissolved CO_2 or else, aqueous CO_2, $CO_2(aq.)$ is found in two forms. The hydrated form $H_2CO_3^\circ$, and the non-hydrated form CO_2°. As we know, CO_2 dissolution leads to acidification of the brine, which is of interest in fluid-rock interactions and depends on the CO_2 solubility. In the table below (Table 5), a summary of the solubility models used by the selected simulator of this thesis can be found.

Simulator	Solubility Model	Temperature (°C)	Pressure (bar)	EOS (Fugacity Calculation)
GEM	Henry's Model	up to 150	1 - 700	Modified Redlich -Kwong [59], or Peng - Robinson [60]
	Modified Henry's constant model [58]	up to 150	1 - 700	Fugacity of gaseous components soluble in the aqueous phase calculated by Li and Nghiem [61]
	Modified Henry's constant model based on internal ENI experimental data.	up to 150	1 - 1100	

Table 5: Specifications of the selected simulator.

4.6 Standards for selecting a geochemical code

First and foremost, no simulator today meets all of the criteria to be considered the optimal one. Simulators are chosen based on the most critical factors for a specific scenario and the objective of a particular study. Nevertheless, those chosen in this study are some of the most frequently used commercial simulators available to date.

The criteria for the selection of the simulators in terms of features include the following:

- Code availability.
- Code documentation.
- Code support.
- Ability to handle both equilibrium and kinetic modelling approaches.

- Include an adequate activity model.
- A thermodynamic and kinetic database that can be accessed from within the program.
- Capability to handle multi-phase flow.
- Capability to deal with the heterogeneity of medium.
- Computational performance that is both efficient and robust.
- Capability to model CO_2 solubility with high precision.
- Capability to model reactive transport.
- Capability to model diffusion.

CHAPTER 5

FLUID FLOW MODELLING AND SIMULATION OF CARBON STORAGE

5.1 Introduction

To fully understand the reservoir's response to the injection of CO_2 and to simulate its long-term containment, fluid flow modelling is necessary and is considered part of the typical workflow of a reservoir study. In almost every case, alongside the routine fluid flow analysis, a coupled geomechanical model is also built.

The development of a CCS project heavily relies on fluid flow modelling and simulation. CO_2 storage involves flow and transport phenomena in porous media that occur on different spatial and temporal scales [63]. As a result, physically accurate numerical simulations with high resolutions are required to effectively predict where CO_2 will likely flow, interpret the volume and spatial distribution of CO_2 on a large scale, and optimize injection operations into geological formations. In particular, species diffusion and viscous fingering are two examples of transport phenomena that take place at small scales, whereas CO_2 storage occurs at macroscales that can extend over several kilometers and many years. Regarding the adequate computational approach that needs to be followed, a fine grid model is a necessity, to resolve the coupling between flow and phase behavior.

In terms of the CO_2 injection forecasting models, they can be divided into two categories, screening models and simulation models. Screening models are simple models that are generally used to estimate the potential increase in hydrocarbons' recovery and the maximum amount of CO_2 that can be stored if CCS activities are continued beyond the hydrocarbons' recovery stage. While such screening models assume that the reservoir structure is homogenous, this is not always the case. Simulation models, on the other hand, take into account reservoir heterogeneities. Simulation models are further divided into black oil models which assume homogeneous composition of oil, and compositional models which predict the fluid's behavior according to its components as well as their interactions. In CCS projects compositional models are selected since CO_2 alters oil's characteristics, such as viscosity, volume, and miscible pressure [64]. Some commercial simulators available in the market today are Eclipse 300 by Schlumberger, GEM by CMG and, ToughReact [65] by the Lawrence Berkeley National Laboratory. The one selected for this thesis was decided to be CMG's GEM because of its capability to simulate large-scale systems such as depleted reservoirs and aquifers and well-established geochemical modules.

5.2 Fluid flow modelling in porous media, theory and fundamental governing equations

Geological storage of carbon dioxide requires the study of complex physicochemical processes, which involve flow and transport phenomena in porous media alongside slow chemical reactions. All relevant physical and chemical processes, as well as the primary and secondary trapping mechanisms, must be included in the theoretical description of the storage. Furthermore, it is necessary to also account for CO_2 and geological media properties. Considering that carbon storage takes place over long periods and involves a plethora of mechanisms, we can understand it adds significant complexity to theoretical modelling, and numerical simulation typically used for reservoir engineering [50].

The physical model used most frequently for the flow of a fluid through a porous medium is Darcy's law. Henry Darcy formulated the law based on the outcome of experiments involving the flow of water through sand beds [66].

$$\mathbf{q} = -\frac{\mathbf{k}}{\mu}(\nabla p - \rho \mathbf{g}) \tag{1}$$

where **q** is a vector representing discharge per unit area in a three-dimensional system, with velocity as the unit. The permeability tensor **k** represents the ability of the medium to transmit fluids through the pore spaces, **q** is not the velocity which the fluid travelling through the pores is experiencing, but it can be linked to the pore (interstitial) velocity through the porosity ϕ of the medium.

$$\mathbf{v} = \frac{\mathbf{q}}{\phi} = -\frac{\mathbf{k}}{\mu\phi}(\nabla p - \rho \mathbf{g}) \tag{2}$$

A three-dimension Cartesian coordinate system can be used to account for anisotropy in the medium's symmetric permeability tensor, which is given by:

$$\mathbf{k} = \begin{pmatrix} k_{xx} & k_{xy} & k_{xz} \\ k_{xy} & k_{yy} & k_{yz} \\ k_{zx} & k_{zy} & k_{zz} \end{pmatrix}, \text{ where } k_{ij} = k_{ji}.$$

Employing Darcy's law in carbon storage requires an extension of the equation to account for the phases involved, such as brine, solid, and carbon dioxide. Nevertheless, the equations are similar to those used to describe oil, water, and gas flowing through conventional porous reservoirs. In multi-phase flow, the equation is applied for every phase, by replacing the permeability with effective (phase) permeability. This approximation is valid under steady-state conditions. In addition, the definition of relative permeability shows the ability of each flowing phase to flow when mutual interactions exist among them. Considering the positive z-direction is upwards and opposite to gravity, Darcy's equation extended for each fluid phase, can be expressed as follows:

$$\mathbf{v}_i = \frac{\mathbf{q}_i}{\phi} = -\frac{\mathbf{k}\, k_i}{\mu_i \phi}(\nabla p_i + \rho_i g \nabla z) \tag{3}$$

If the flow of a multi-phase, multi-component system is to be modeled, Darcy's equation needs to be coupled with conservation of mass and energy equations. Depending on the case, the number of system components and phases taken into account can be different. The conservation of mass is expressed by the balance of four terms comprising all possible mechanisms of mass transfer, which are the time rate of change of mass at a fixed point, or the local derivative or storage term, convective and diffusive transports, and source/sink term of mass. Similarly, energy conservation is analogous to mass conservation expressed by the balance between the time rate of change of energy, energy storage in fluid phases and matrix, convection or advection, conduction, as well as possible source/sink terms [50]. By assuming regional thermal equilibrium since flow velocities are small, and insignificant dissipative effects, the energy conservation equation is greatly simplified.

These fundamentals equations governing the numerical simulation of carbon storage also involve properties of the multi-phase fluid (viscosity, density), geomechanical effects (porosity of the solid rock matrix), as well as possible contributions from the geochemical reactions, which all have an effect on flow and transport behavior [67]. Furthermore, additional constraints for saturation levels

$$\Sigma S_i = 1 \tag{4}$$

pressures,

$$P_c = P_{non\ wetting} - P_{wetting} \tag{5}$$

and component compositions, must be added to the equations governing the process. Lastly, it has also been observed that impurities in the CO_2 composition may affect carbon storage. The use of equation of state models (EOS) to calculate CO_2 mixtures densities has been considered of paramount importance during modelling and simulation of CCS [68].

Fluid property	Dependence
ρ_{CO_2}	$f(\mathrm{T},\mathrm{p})$
H_{CO_2}	$f(\mathrm{T},\mathrm{p})$
μ_{CO_2}	$f(\mathrm{T},\mathrm{p})$
ρ_{brine}	$f(\mathrm{T},\mathrm{p},S,\mathrm{X}_{water}^{CO_2})$
H_{brine}	$f(\mathrm{T},\mathrm{p},S,\mathrm{X}_{water}^{CO_2})$
μ_{brine}	$f(\mathrm{T},S)$

Table 6: Fluid properties dependence of CO_2 and water in a carbon-brine system [50].

5.3 Limitations and challenges in numerical modelling

It is now clear that numerical simulation of the CO_2 injection in a geological storage is a challenging task due to the inclusion of multiple phases and components. Flow and transport of the flowing phases, as well as geomechanical effects and geochemical reactions, must be considered in the mathematical models employed in the simulators. As a consequence, the simulator's accuracy is strongly sensitive to the choice of data- especially to the fluid properties, kinetic modelling solutions of the geochemical reactions, and the geological input. Also, these input parameters can play different roles depending on the simulation type. Geochemical modelling, for example, will be less crucial in short-term simulations (i.e., less than 100 years after the initial injection). On the other hand, it will become more relevant in long-term simulations.

All of this raises the complexity of the mathematical problems and the frequency of numerical concerns faced when solving these equations, resulting in restrictions and uncertainties in the mathematical formulations. Specifically, the momentum balance based on the multi-phase extension of Darcy's law is a notable constraint of the mathematical formulations. Darcy's law for single-phase flow has been derived from fundamental principles under assumptions substituting momentum conservation equations, such as Navier-Stokes. Therefore, its application to multi-phase, multi-component systems is not rigorous, thereby limiting its potential. Nonetheless, Darcy-like equations seem to be prevalent, and they are almost always used in the oil and gas industry since different methods are not yet well established in the sector. Implementation of the traditional formulation is largely determined by the adequacy of the continuum approximation, the validity of Darcy's equation and its extension to multi-phase flow, and the appropriate mathematical models for relative permeability [69].

5.4 Geological carbon storage simulators features

The simulation of CO_2 storage is a particularly challenging task because of the broad range of time and length scales involved, and since analytical solutions of the governing equations are unavailable. In addition, because the governing equations are non-linear partial differential equations, along with the discretization in both time and space, they pose a computationally challenging issue. When it comes to discretization in time and space, precision, stability, and computational speed are the most important parameters to be considered.

The simulators used nowadays for carbon storage simulation were generally derived from codes used in the petroleum industry for multi-phase flow in porous media, both taking into account geochemical reactions or not. Simulators differ between them according to their modelling approximations, discretization schemes, and numerical accuracy, but are related by the type of numerical method they use. It is possible to classify numerical methods used by the simulators into three main categories, finite difference, finite element, and finite volume. So far, all three have been utilized in the petroleum industry. Depending on how many fluid phases and components are considered, as well as the discretization methods used, the complexity of the simulators varies considerably. The following table (Table 7) presents the main applications and numerical features of the selected simulator of this thesis used in the next chapter.

Simulator	Main application	Numerical features
GEM	Multidimensional, equation-of-state (EOS) compositional reservoir simulator [71].	GEM can be run in explicit, fully implicit and adaptive implicit modes.
	Simulation of all mechanisms of a miscible gas injection process.	The quasi-Newton successive substitution method, QNSS, as developed at CMG, is used to solve the nonlinear equations associated with the flash calculations.
	Includes CMG Results, a visualization software that is used to examine 2D and 3D reservoir properties, as well as XY plots of dynamic data.	GEM uses AIMSOL, which is a state-of-the-art linear solution routine, developed especially for adaptive implicit Jacobian matrices.

Table 7: Overview of the selected simulator for CCS.

The utilization of the integrated finite difference method (IFDM) has the advantage of being able to achieve high-order accuracy without the need for unnecessarily complex formulations. Additionally, it can be used to solve partial differential equations in complex domains. This is particularly useful for CCS simulations that involve domain or phase variations, such as those that occur during fluid phase migration [50].

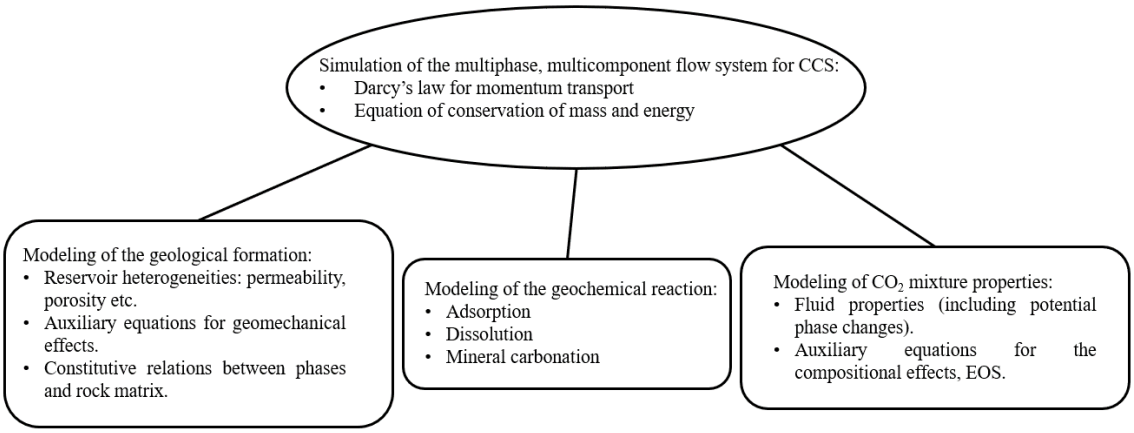

Fig. 10: Schematic of physical modelling of CCS.

CHAPTER 6

SIMULATION OF A CO_2 STORAGE USING A COMMERCIAL SIMULATOR

6.1 Introduction

The commercial geochemical simulator used in this thesis is Computer Modelling Group's (CMG) GEM and comes as part of CMG's software suite. Among the available tools of the suite, the ones used are:

- Pre-processor (Builder)
- Post-processor (Results).
- Fluid characterization and phase behavior software (WinProp).

The version used was 2021.10, in which a new CCS process wizard was implemented within Builder that helps build data sets using various trapping mechanisms by putting all inputs in one place.

6.2 Dry gas reservoir base model set up

The data used to describe the reservoir came primarily from the literature, and were based on case studies that describe how reservoirs were effectively turned into CO_2 storages. As mentioned previously, the porosity and permeability of reservoirs appropriate for CO_2 storage are high, allowing injected CO_2 to displace the fluid in the host rock and fill the pore space. Furthermore, the reservoirs must have a high enough pressure and temperature that the stored CO_2 is in a supercritical condition, maximizing storage capacity.

Also, there is a variety of options in terms of the possible CO_2 injection sites, but in this study, modelling was performed on a dry gas reservoir.

6.2.1 Reservoir dimensions and thermodynamic and physical properties

The simulated reservoir is actually a simplified case, corresponding to a parallelepiped of relatively small extension (250x250 m^2), mimicking a homogeneous porous volume subject to production and then CO_2 injection through a producing well and an injector well. Because of this simplified reservoir geometry results can be considered unaffected by the shape or layering of the geological formation. The number and dimensions of the grid's cells are 25 cells of 10 m (I-direction) × 25 cells of 10 m (J-direction) in the horizontal plane × 16 cells of 5 m (K-direction) in the vertical direction. In total, the reservoir comprised 10.000 blocks which was the academic license's limit.

The simulated model is shown in fig. 11.

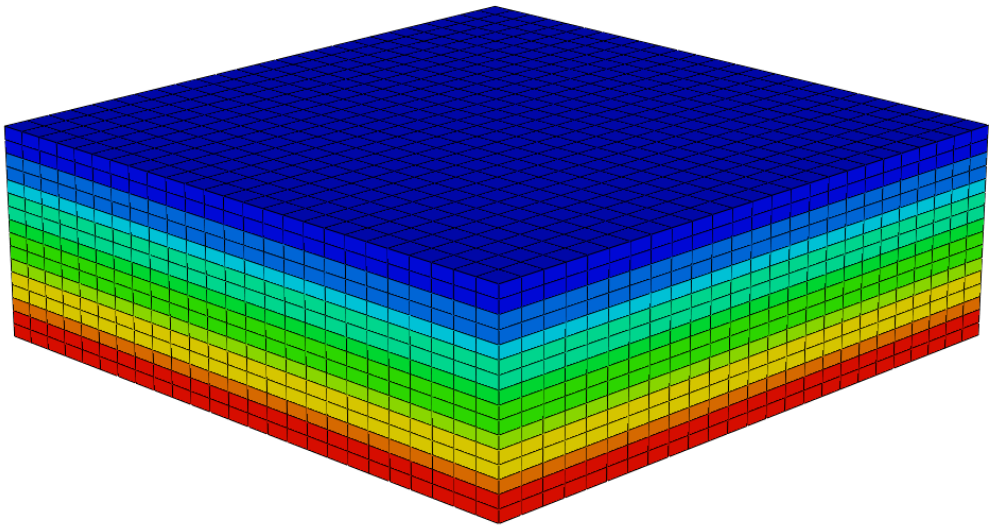

Fig. 11: Reservoir's geometry grid (250m×250m×80m).

The system properties are summarized in table 8.

Property	Value
Temperature (°C)	50
Pressure (bar)	150
Porosity (%)	20
Permeability (md)	100
Rock Compressibility (1/kPa)	7.25E-7
Length (m)	250
Width (m)	250
Thickness (m)	80
Depth (m)	1500

Table 8: Overview of the selected reservoir's physical properties.

6.2.2 Reservoir fluid model properties

The compositional EOS fluid model selected was the industry's default option, the Peng-Robinson (1978) model.

In terms of the composition of the reservoir, it was assumed the reservoir consists of only 3 components, methane (CH_4), carbon dioxide (CO_2), and brine.

The original species concentrations were based on typical brine data from the literature, and were equal to:

- $Na^{+} = 30000\,ppm$
- $Ca^{2+} = 500\,ppm$
- $Al^{3+} = 1\,ppm$
- $SiO_2 = 181\,ppm$

A value for $pH = 7$ was also set.

Regarding water compressibility c_w, it was set equal to 2.9E-7 1/kPa, with an irreducible water saturation of S_{wi} 30%.

6.2.3 Reservoir rock composition

The minerals that were considered to be present in the reservoir, and their corresponding initial volume fractions with respect to the bulk rock volume were:

- Calcite, V=0.0088
- Kaolinite, V=0.0176
- Anorthite, V=0.0088

and the corresponding mineral/solid reactions were:

- Calcite: $CaCO_3 + H^+ = Ca^{2+} + HCO_3^-$
- Kaolinite: $Al_2Si_2O_5(OH)_4 + 6H^+ = 2Al^{3+} + 5H_2O + 2SiO_2$
- Anorthite: $CaAl_2Si_2O_5O_8 + 8H^+ = 2Al^{3+} + 4H_2O + Ca^{2+} + 2SiO_2$

6.2.4 Reservoir rock-fluid properties

The relative permeability curves can be generated using built-in correlations, the Corey functions [72] that are based on end-points, or can be inserted by the user from any other source.

In this case, the relative permeability curves and the value for the critical gas saturation S_{gc} =0.08 of the In-Salah Gas Krechba Field CCS in Algeria were used [73].

S_g	k_{rg}	S_w	k_{rw}
0	0	0.3	0
0.08	0	0.38	0.00015
0.16	0.000407	0.46	0.002439
0.23	0.005831	0.53	0.012346
0.31	0.024131	0.61	0.039018
0.39	0.064892	0.69	0.09526
0.47	0.140566	0.77	0.197531
0.54	0.269314	0.84	0.36595
0.62	0.484797	0.92	0.624295
0.7	1	1	1

Table 9: Relative permeability curves.

6.2.5 Wells definition and properties

Two production – injection scenarios were implemented to assess the impact of production history, consisting of 2 wells, one producer and one injector. For both scenarios the simulations last 200 years with the monitoring period substantially longer than the injection time in order to explore variations in the CO_2 distribution in the reservoir. Specifically, for the first scenario:

- Production lasts for 1 year, from 01-01-2020 to 01-01-2021. Then the well is shut in, and CO_2 injection takes place right after the production phase, from 01-01-2021 to 01-01-2022, when the injector gets shut in too.

Then for the second scenario:

- Production lasts for 2 years, from 01-01-2020 to 01-01-2022, and then, CO_2 injection lasts for another 2 years, from 01-01-2022 to 01-01-2023.

In the first scenario the natural gas rate was equal to 75.000 m^3/day and the CO_2 injection was equal to 75.000 m^3/day. In the second scenario, the production rate remained unchanged, whereas the injection rate was increased by 25%, to 93.750 m^3/day.

The location and perforation interval were the same for both scenarios. The perforations were defined towards the bottom of the reservoir.

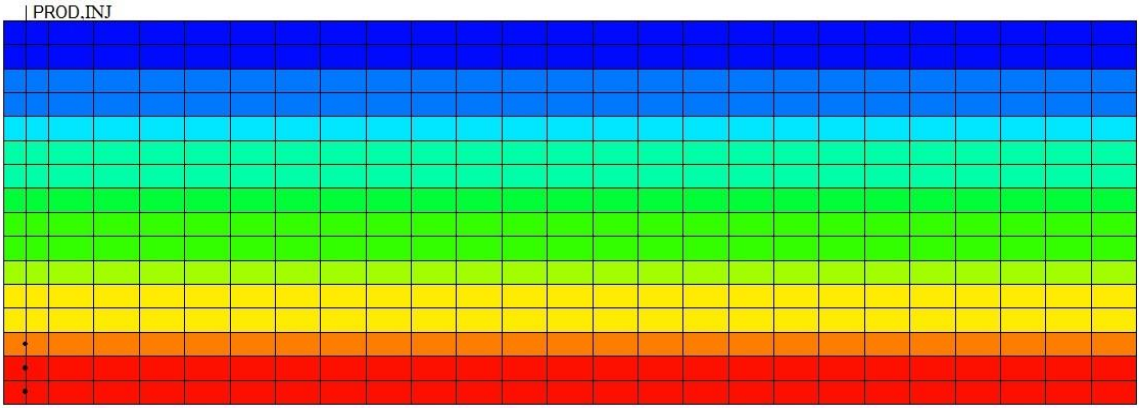

Fig. 12: Perforation interval for producer and injector (blocks 1 1 14:16).

6.3 Simulation strategy

The basic 3-dimensional reservoir model and compositional fluid model served as the basis for all subsequent simulations.

The simulation strategy was aimed at assessing the impact of each trapping mechanism on the CO_2 distribution in the stored volume. Therefore, structural trapping, capillary trapping, solubility trapping, mineral trapping and water vaporization were progressively taken into account by subsequent simulations.

6.4 Scenario 1: presentation of simulation results

6.4.1 Base model with structural trapping

The well bottom-hole pressure and trapped & cumulative injected CO_2 are shown in fig. 13 and 14, respectively.

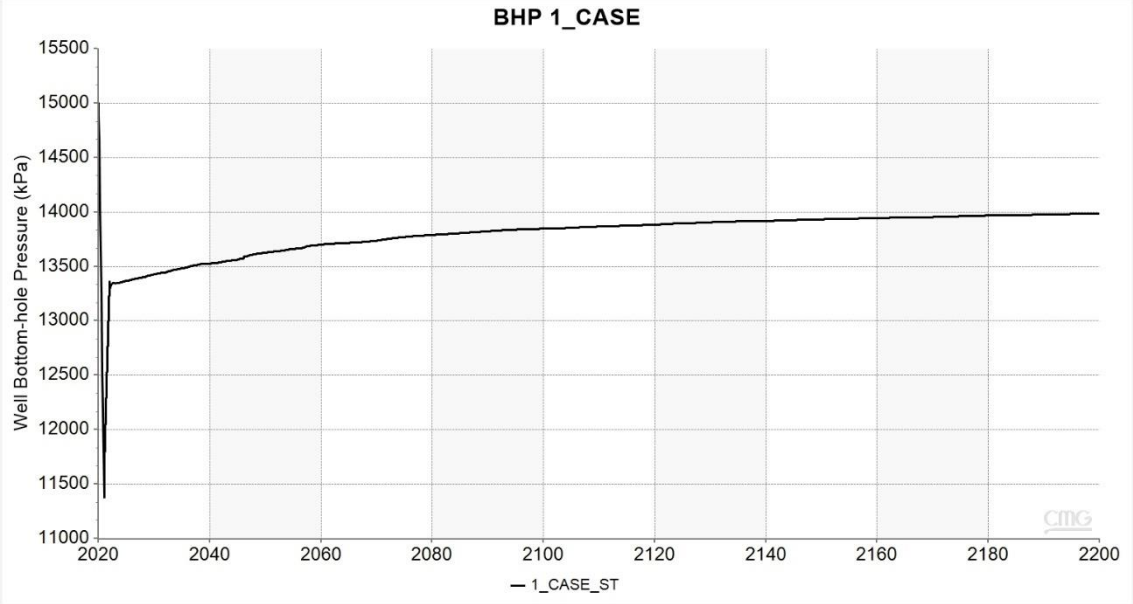

Fig. 13: 1_Case: Bottom hole pressure (BHP).

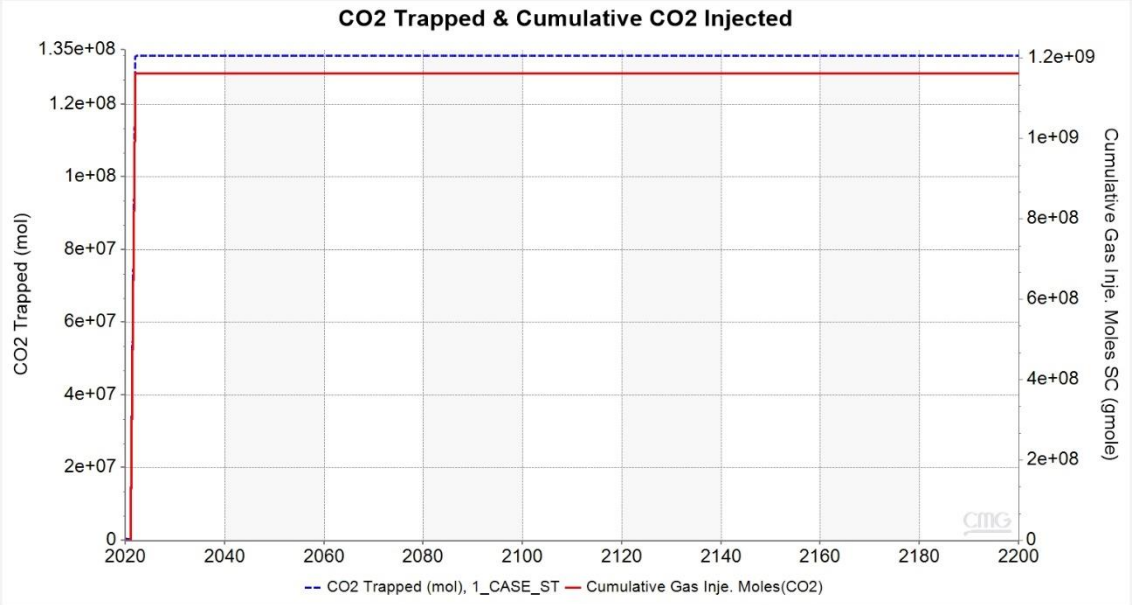

Fig. 14: 1_Case: CO_2 trapped & cumulative CO_2 injected.

From figure 14, it can be observed, that the total CO_2 injected is equal to 51.112.000 kg (1.16E+9 moles), while the amount of CO_2 trapped by capillary trapping is equal to 5.868.000 kg (1.34E+8 moles). The rest of CO_2 remains in the reservoir in supercritical phase.

1_Case	Total CO_2 Injected	51.112.000 kg	Trapped % of total CO_2
	Capillary trapping	5.868.000 kg	**11.5**

Table 10: 1_Case: % of total injected CO_2 trapped.

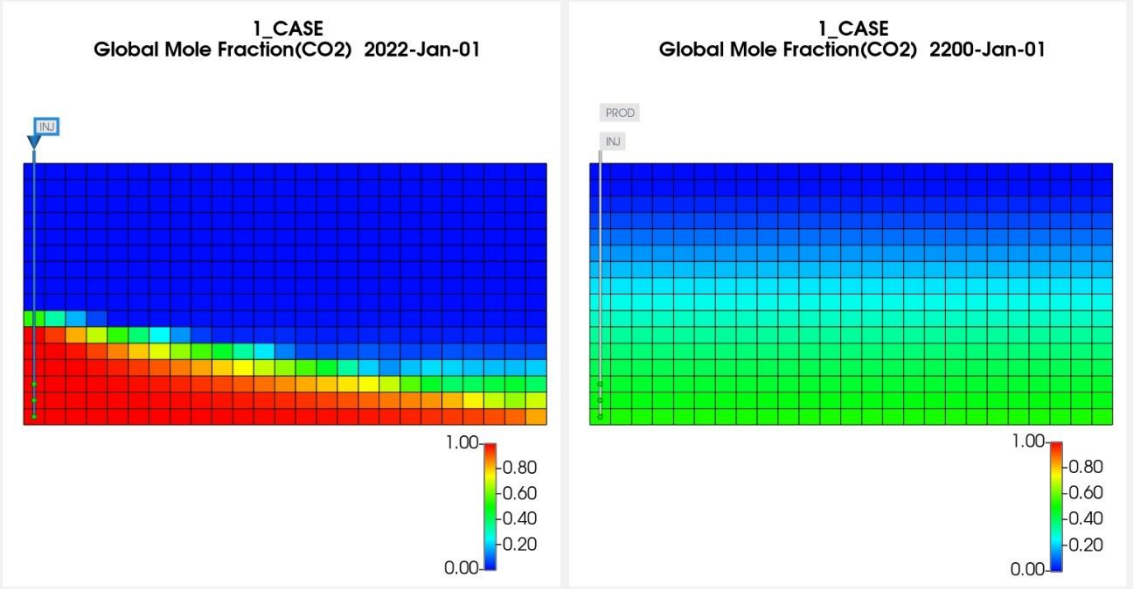

Fig.15: 1_Case: CO_2 global mole fraction right after injection and at the end of simulation.

Looking at the global mole fraction, we can see that CO_2 being a heavier phase than CH_4, initially accumulates at the bottom of the reservoir. However, over time, CO_2 es in the reservoir (Figure 15).

6.4.2 Model with structural trapping, solubility and capillary trapping

In the second case, the prior model's structural trapping is extended to account for solubility and hysteresis (capillary) trapping. In solubility trapping, CO_2 is trapped by changing its composition in the aqueous phase at specific pressures and temperatures. As a result, pressure, temperature, and surface area contact with an aqueous phase, are all critical factors in solubility trapping.

To trap the non-wetting phase, the hysteresis trapping employs the relative permeability curves defined for drainage and for imbibition. The used hysteresis model is a linear hysteresis model with no distinction on the direction of saturation change. Regarding gas phase (CO_2) trapping, the Land [74] model was applied. However, the effect of hysteresis trapping is expected to be very limited as CO_2 is injected in a depleted gas reservoir where water corresponds to the formation water.

The impact of the value of maximum residual gas saturation was investigated in the second case of the first scenario by using two different values, the software's default value and equal to the critical gas saturation of the In-Salah field.

6.4.2.1 Default value for maximum residual gas saturation

For the first simulation of the second case, the software's default value for maximum residual gas saturation was used and it was equal to the mid-point between S_{gc} and $1\text{-}S_{wi}$.

$$S_{gr,\max} = 0.31$$

The solubility model used is a modified version of the Henry's constant correlations to give improved results for CO_2 based on internal ENI experimental data (HENRY-MOD1-CO2).

The well bottom-hole pressure and trapped & cumulative injected CO_2 are shown in fig. 16 and 17, respectively.

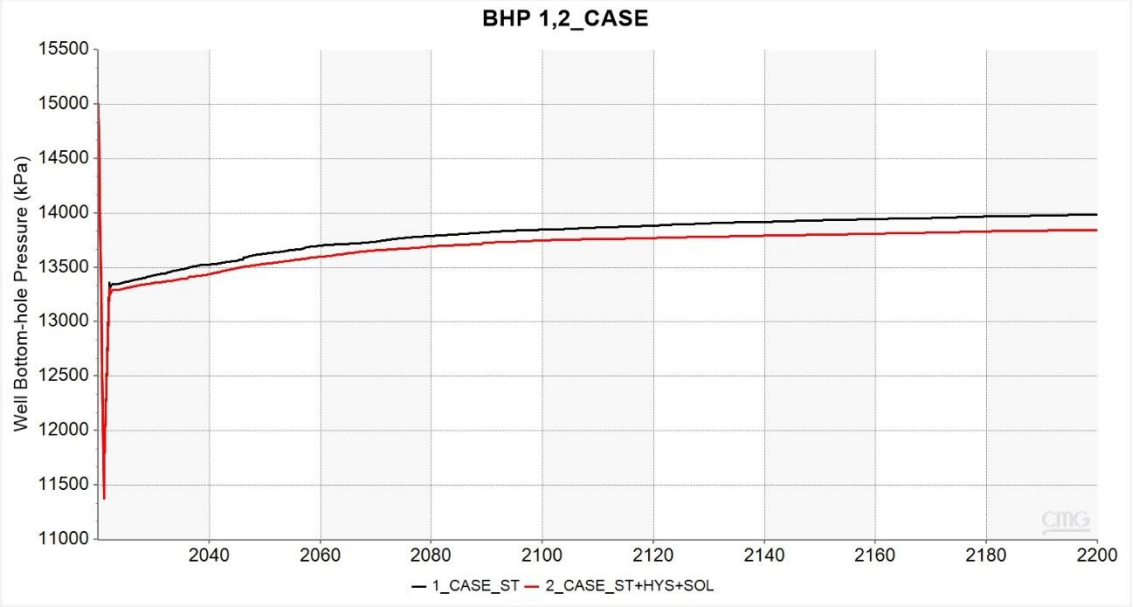

Fig. 16: 2_Case Bottom hole pressure (BHP).

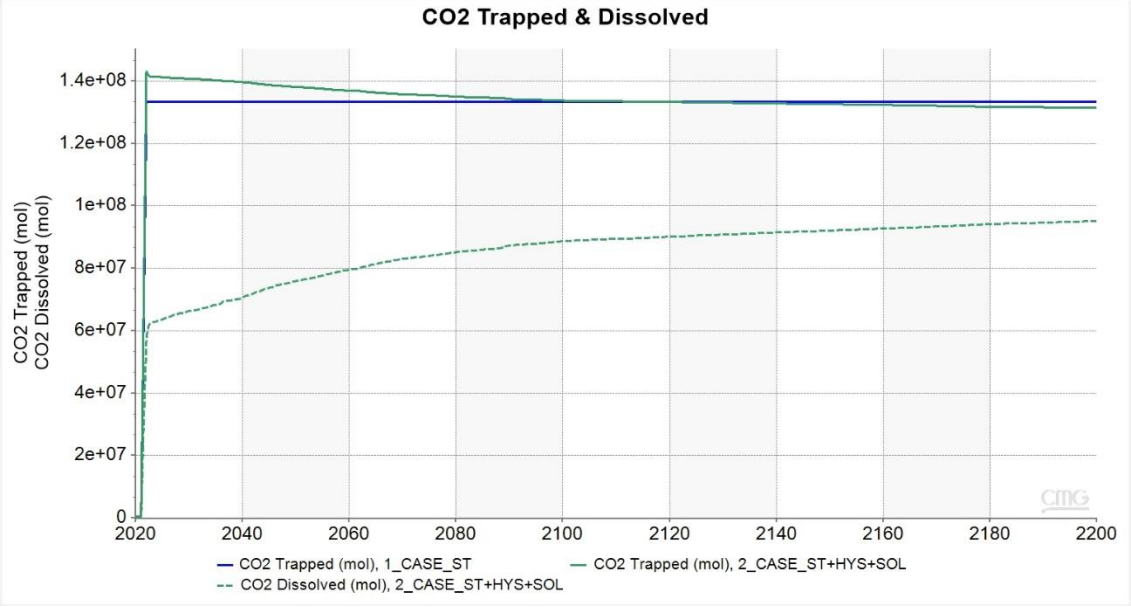

Fig. 17: 2_Case: CO_2 trapped, dissolved, and comparison with 1_Case.

Looking at figure 17, the amount of CO_2 trapped by structural and hysteresis trapping is less than in the first case where only structural trapping was considered. Although, there is an additional amount of CO_2 trapped by solubility trapping. The feature of a gradual decrease of CO_2 trapped is more apparent in this case since some of the CO_2 also gets soluble over time in the aqueous phase.

2_Case	Total CO_2 Injected	51.112.000 kg	Trapped % of total CO_2
	Capillary trapping + hysteresis	5.782.000 kg	11.3
	Dissolved in water	4.189.000 kg	8.2
	Total CO_2 trapped	9.971.000 kg	**19.5**

Table 11: 2_Case: % of total injected CO_2 trapped.

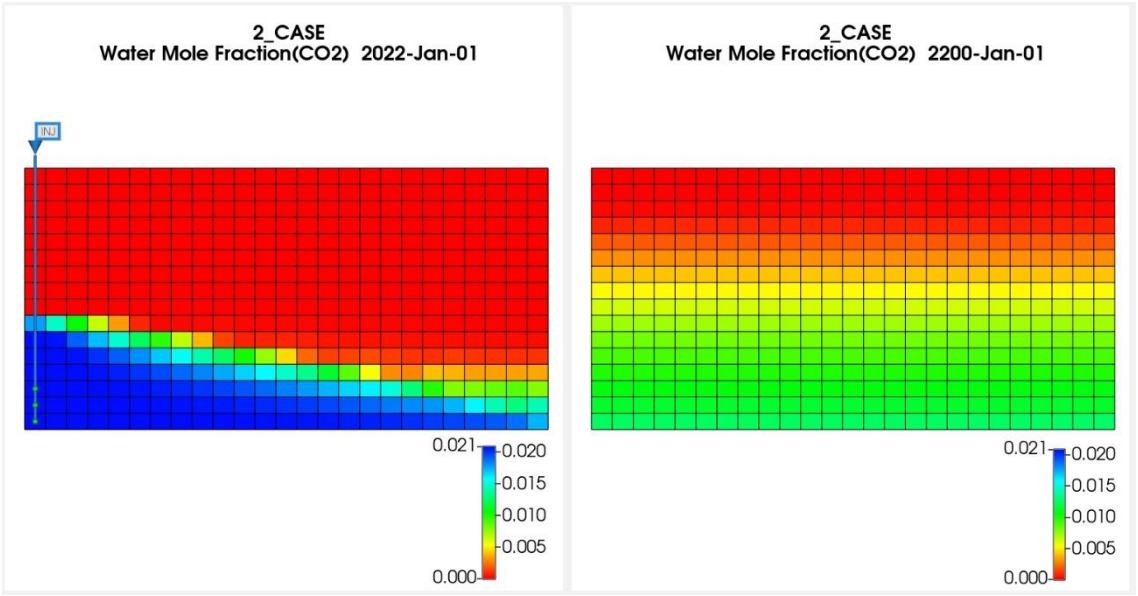

Fig. 18: 2_Case: CO_2 water mole fraction right after injection and at the end of simulation.

As can be seen from the above table 11, the amount of CO_2 trapped by solubility is significant and accounts for an additional 8.2% of the total CO_2 injected. Conversely, as expected in the case of a depleted gas reservoir, the CO_2 by structural trapping in the first case, and CO_2 trapped by structural plus capillary trapping in the second case are almost equal.

Also, looking at the water mole fraction of CO_2 from figure 18, we can see that CO_2 gets dissolved in water together with its gradual dispersion in the reservoir.

Due to the additional amount of CO_2 trapped in the second case, as seen from figure 16, the reservoir equilibrates at a lower pressure than in the first case.

6.4.2.2 Maximum residual gas saturation equal to In Salah's field critical gas saturation

For the second simulation of the second case, the value used for the maximum residual gas saturation, was set equal to the critical gas saturation S_{gc} of the In-Salah field.

$$S_{gr,\max} = S_{gc} = 0.08$$

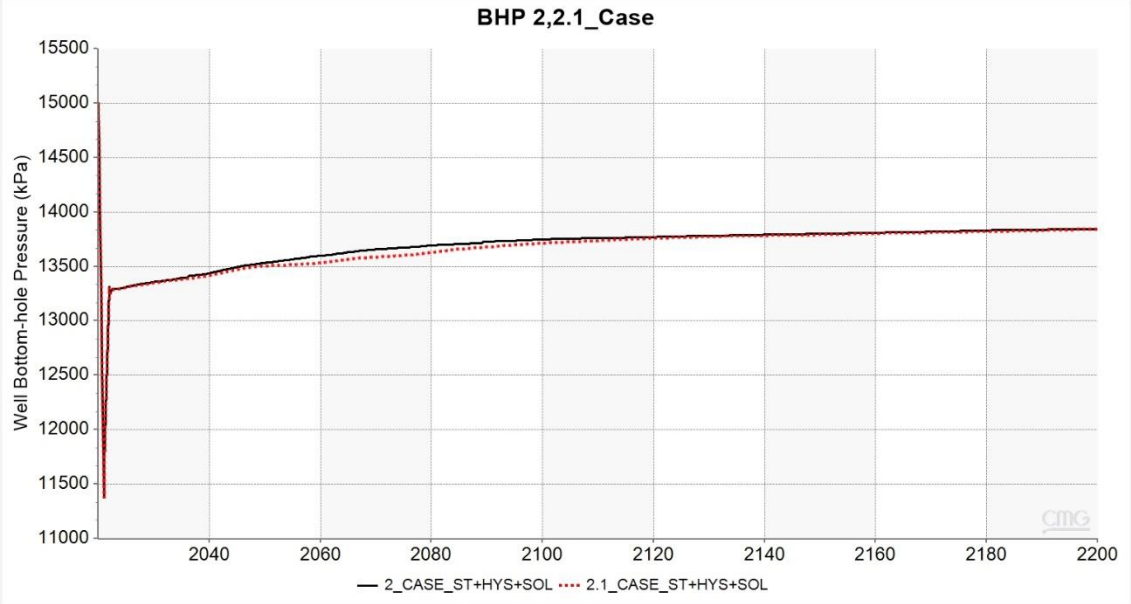

Fig. 19: 2.1_Case: Bottom hole pressure (BHP).

As can be seen from figure 19, the change in the maximum residual gas saturation does not affect the pressure to which the reservoir equilibrates at the end of the simulation. Again, this is due to the CO_2 injection in a depleted gas reservoir.

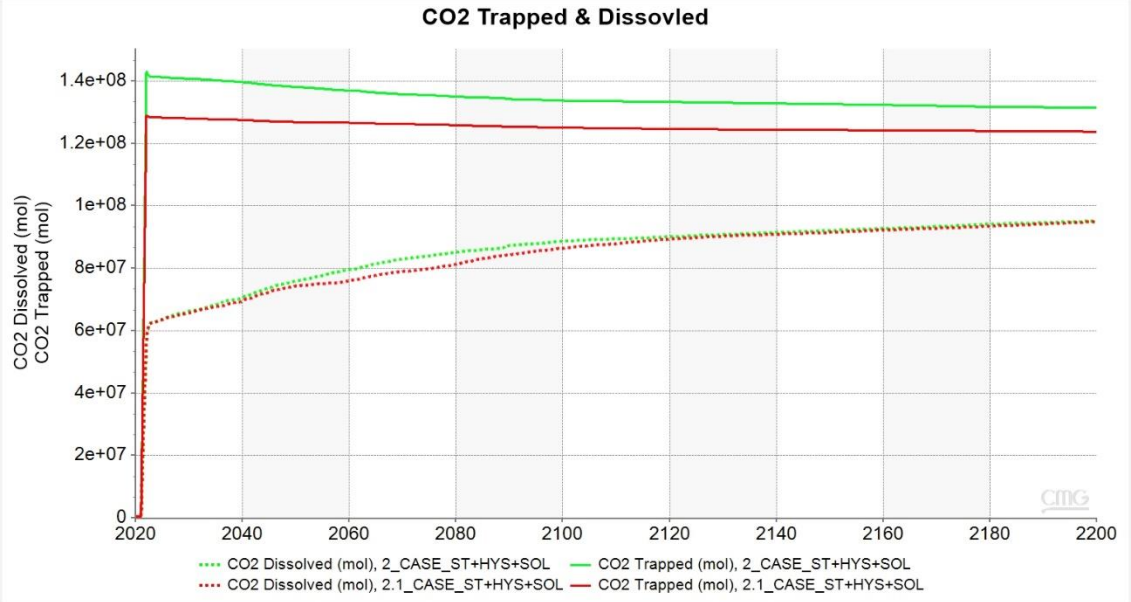

Fig. 20: 2.1_Case: CO_2 trapped, dissolved, and comparison with 2_Case.

Also, no impact on the amount of CO_2 dissolved in water is observed. Nevertheless, the amount of CO_2 trapped by structural and capillary trapping is less in this case, which in turn leads to a lower percentage of the total CO_2 injected. Specifically, the amounts of CO_2 trapped by each mechanism are reported in the following table.

2.1_Case	Total CO_2 Injected	51.112.000 kg	Trapped % of total CO_2
	Capillary trapping		
	+ hysteresis	5.448.000 kg	10.6
	Dissolved in water	4.176.000 kg	8.2
	Total CO_2 trapped	9.624.000 kg	**18.8**

Table 12: 2.1_Case: % of total injected CO_2 trapped.

6.4.2.3 Comparison of different solubility models

Since the amount of CO_2 trapped by solubility trapping is significant compared to the total amount CO_2 injected, two more solubility models available in the software were attempted, using the base 2_case with $S_{gr,max} = 0.31$. First, the Li-Nghiem [75] solubility option, and then by directly inputting Kv-solubility table of CO_2 in water that were generated with WinProp.

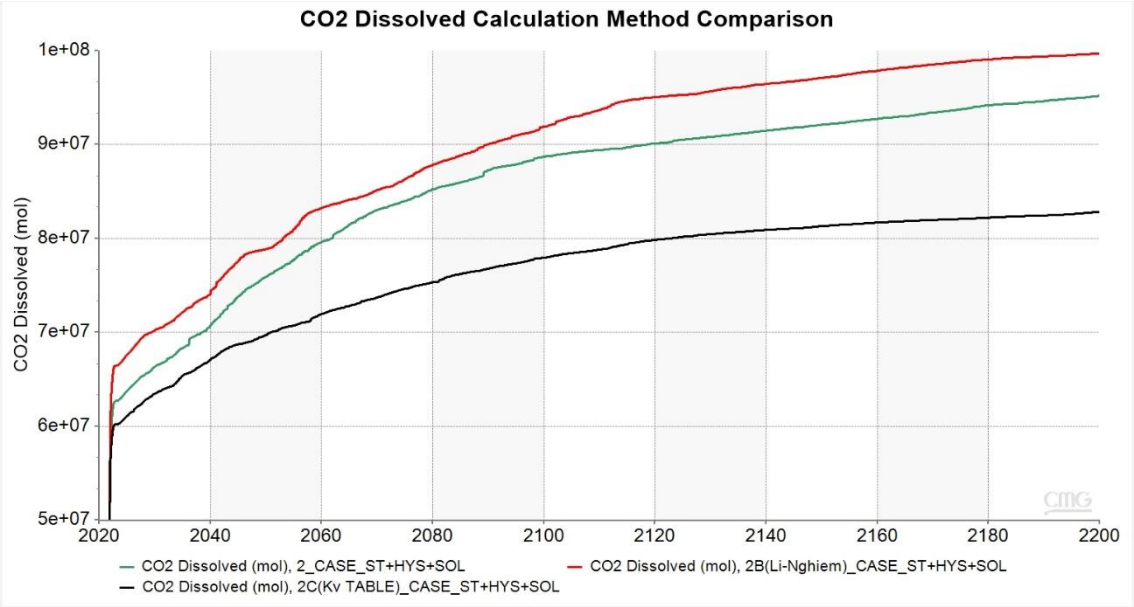

Fig. 21: 2.2_Case: Comparison of CO_2 solubility models.

2.2_Case	CO_2 solubility model	Trapped CO_2
	HENRY-MOD1-CO2 (green)	4.189.000 kg
	Li-Nghiem (red)	4.389.000 kg
	Kv-table (black)	3.645.000 kg

Table 13: 2.2_Case: Amount of CO_2 trapped by different solubility models.

Overall, the results of the 3 solubility models seem to vary. The HENRY-MOD1-CO2 and Li-Nghiem models give close results, with a difference of 5.5%, which is expected in this case, since the temperature is set constant and uniform. The highest difference is of the order or 17% between the HENRY-MOD1-CO2 model and the Kv-table.

6.4.3 Model with structural trapping, solubility trapping, capillary trapping, and mineral trapping

This model builds on the second base case (2_case), which includes capillary and solubility trapping by integrating mineralization due to CO_2.

Mineralization is the safest mechanism of CO_2 trapping, although it takes the longest of the many mechanisms. One explanation for this is that CO_2 must first dissolve in solution before it can be mineralized.

The activity model used to calculate activity coefficients of aqueous species and water, was the B-DOT model by Helgeson [76], an extended method of the Debye-Hückel model.

The aqueous reactions taken into account were:

- $CO_2 + H_2O = H^+ + HCO_3^-$
- $H^+ + OH^- = H_2O$
- $CO_3^{2-} + H^+ = HCO_3^-$
- $CaOH^+ + H^+ = Ca^{2+} + H_2O$

To specify salinity and track salinity variations during the simulation the component of Na^+ was selected.

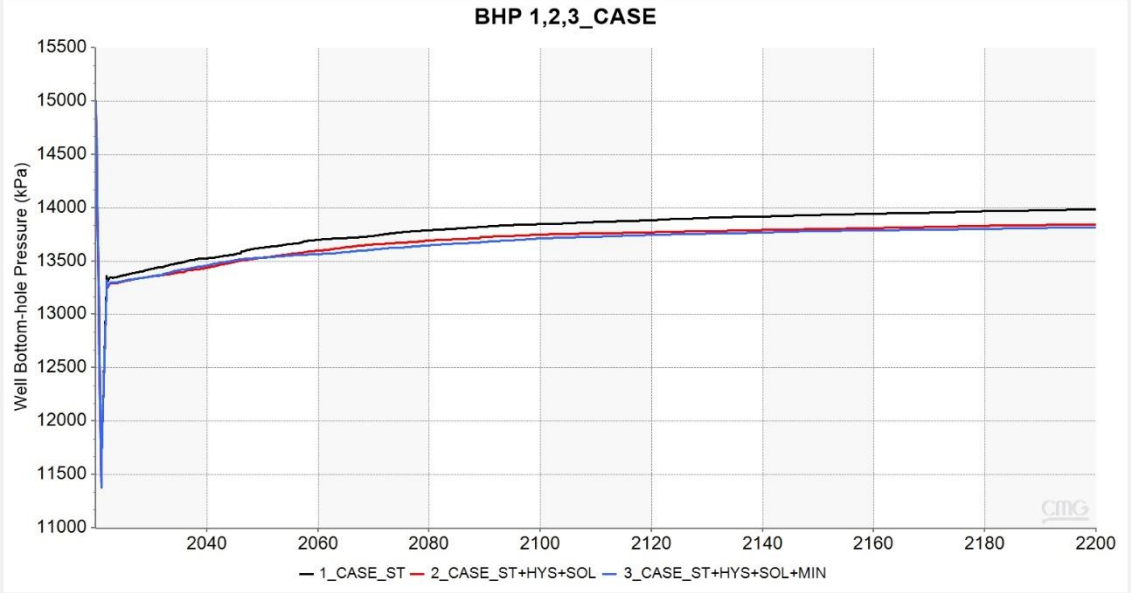

Fig. 22: 3_Case: Bottom hole pressure (BHP).

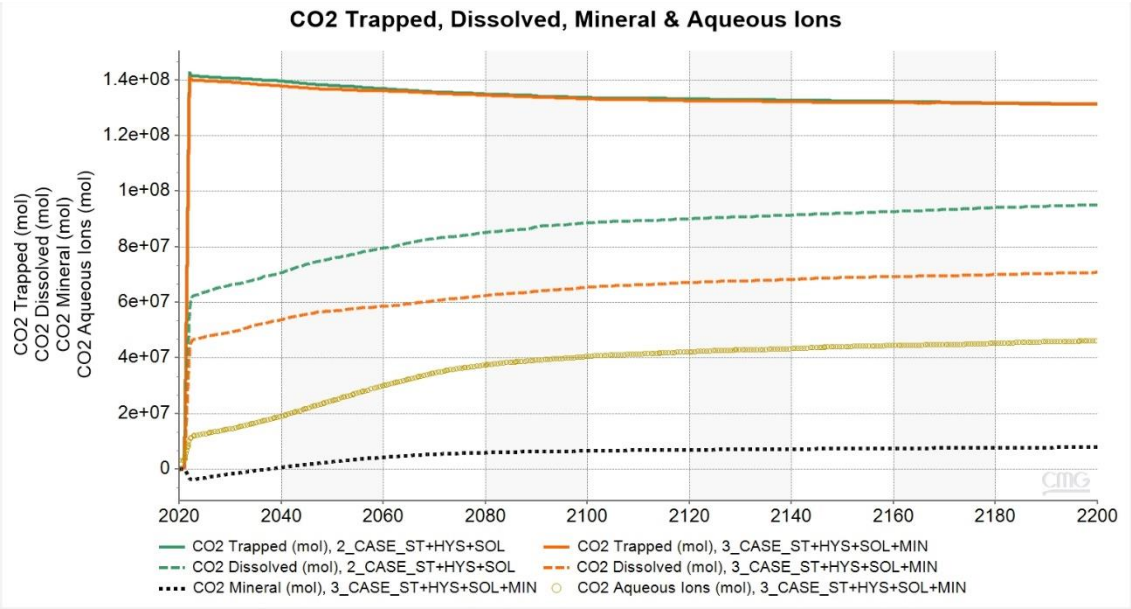

Fig. 23: 3_Case: CO_2 trapped, dissolved, mineral, aqueous ions, and comparison with 2_Case.

By looking at the figure 23, it is obvious that the amount trapped by structural and capillary trapping is the same between case 3, and base case 2. On the other hand, the amount of CO_2 dissolved in water is approximately 25% more on base case 2. However, in case 3, there is an additional amount of CO_2 trapped by mineral trapping or present in CO_2 aqueous ions.

3_Case	Total CO_2 Injected	51.112.000 kg	Trapped % of total CO_2
	Capillary trapping + hysteresis	5.780.000 kg	11
	Dissolved in water	3.116.000 kg	6
	Aqueous Ions	2.036.000 kg	4
	Mineral Precipitate	349.000 kg	1
	Total CO_2 trapped	11.281.000 kg	**22**

Table 14: 3_Case: % of total injected CO_2 trapped.

Looking at the table 14, it is apparent that overall, a larger percentage of the total injected CO_2 is trapped in case 3, in which mineralization is considered. Nevertheless, compared to the base case 2, the difference in the percentage of the total CO_2 trapped is only in the order of +3%.

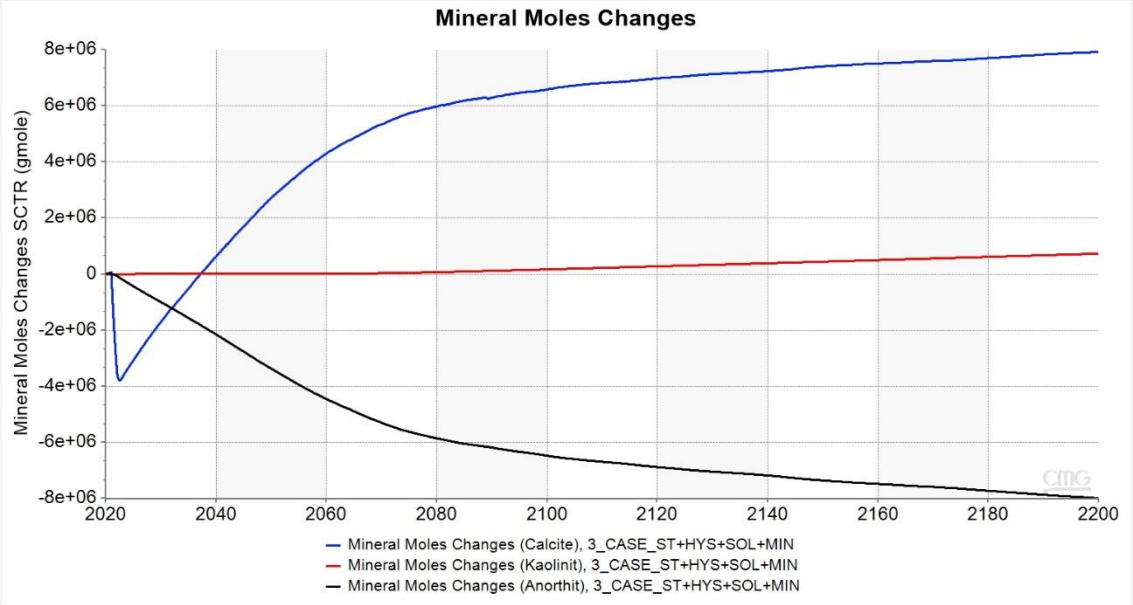

Fig. 24: 3_Case: Mineral mole changes.

Observing the changes in mineral moles, figure 24 shows that during the simulation 'Anorthite' dissolves while 'Kaolinite' slowly precipitates. 'Calcite' though is first rapidly dissolved between 2021 and 2023 and then precipitates.

In figures 25, 26 and 27, the results are visualized with a snapshot of the reservoir for each mineral, at the start and at the end of the simulation.

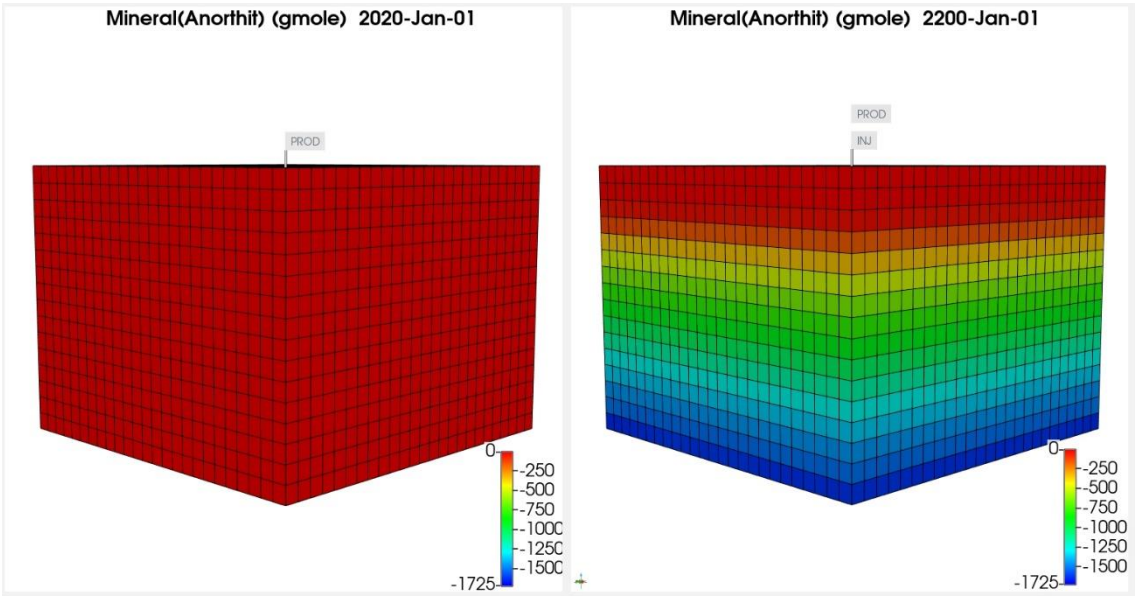

Fig. 25: 3_Case: Mineral mole changes (Anorthite).

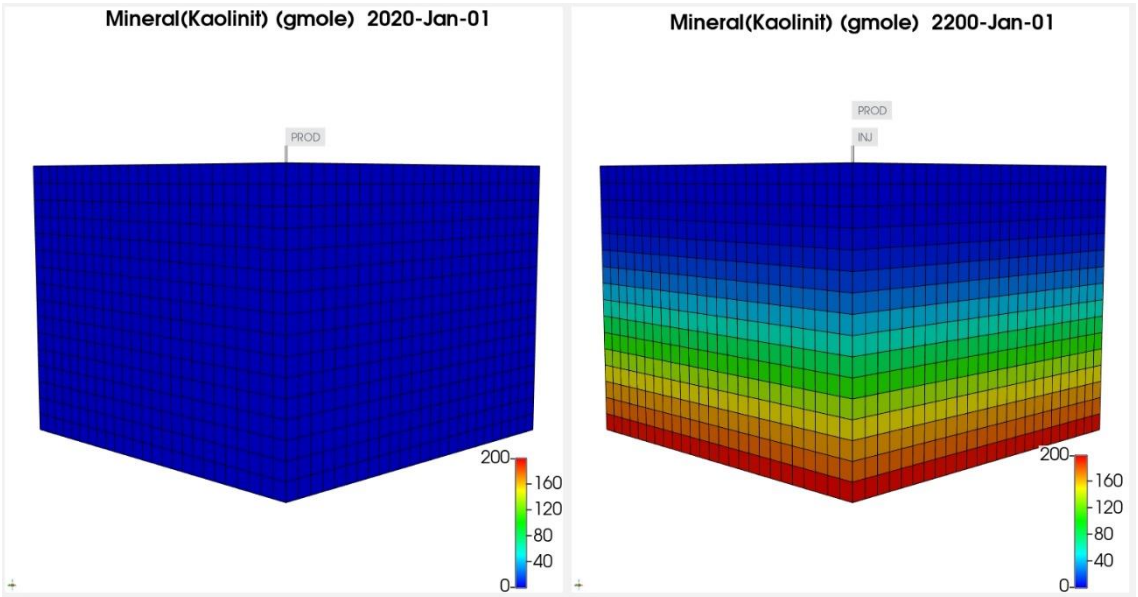

Fig. 26: 3_Case: Mineral mole changes (Kaolinite)

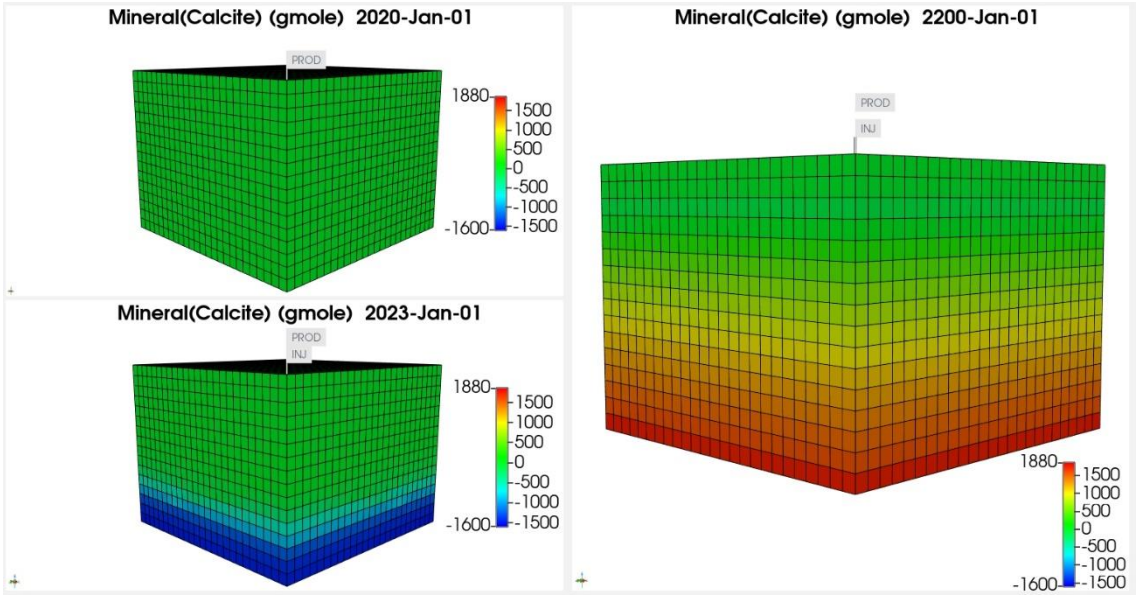

Fig. 27: 3_Case: Mineral mole changes (Calcite).

As expected, the changes in mineral moles mainly take place in the bottom 3 layers where perforations were placed. In general, the effect of CO_2 mineralization does not seem to have a great effect in this simulation, with only about 1% of the total CO_2 injected, trapped in mineral form. In fact, it is known that mineral trapping requires hundreds or even thousands of years to develop, and here a relatively short 180-year duration of the simulation was chosen because of time constraints due to run time.

6.4.4 Model with structural trapping, solubility trapping, capillary trapping, mineral trapping, and water vaporization

This model was built upon the previous case (3_Case) by adding the process of water vaporization around the wellbore, due to high injection pressures of CO_2.

First, a 180-year simulation was run, then additional 1000 years were simulated. The main reason was to investigate if any of the other trapping mechanisms affected the CO_2 distribution in the reservoir and then if in a 1000-year simulation the mineralization has a significant effect on the amount of trapped CO_2.

Figure 28 shows the effect on the bottom hole pressure. Between the fourth and the first case, there is a notable difference, which reaches 5 bar at the end of the monitoring period; a lower static pressure is much desirable because more CO_2 can be injected in the reservoir.

6.4.4.1 180-year simulation

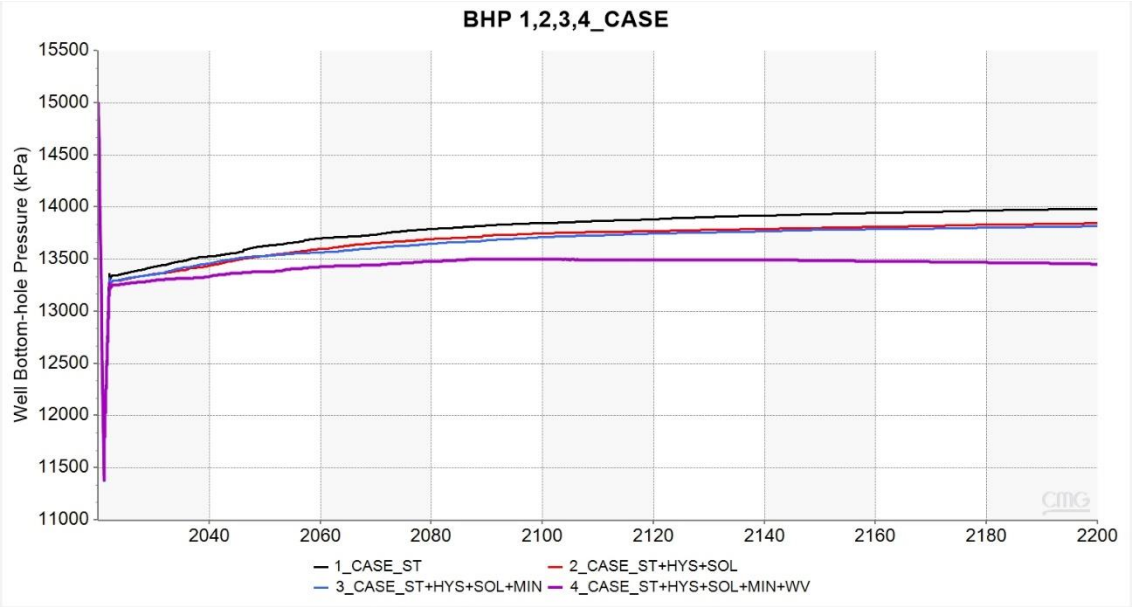

Fig. 28: 4_Case: Bottom hole pressure (BHP).

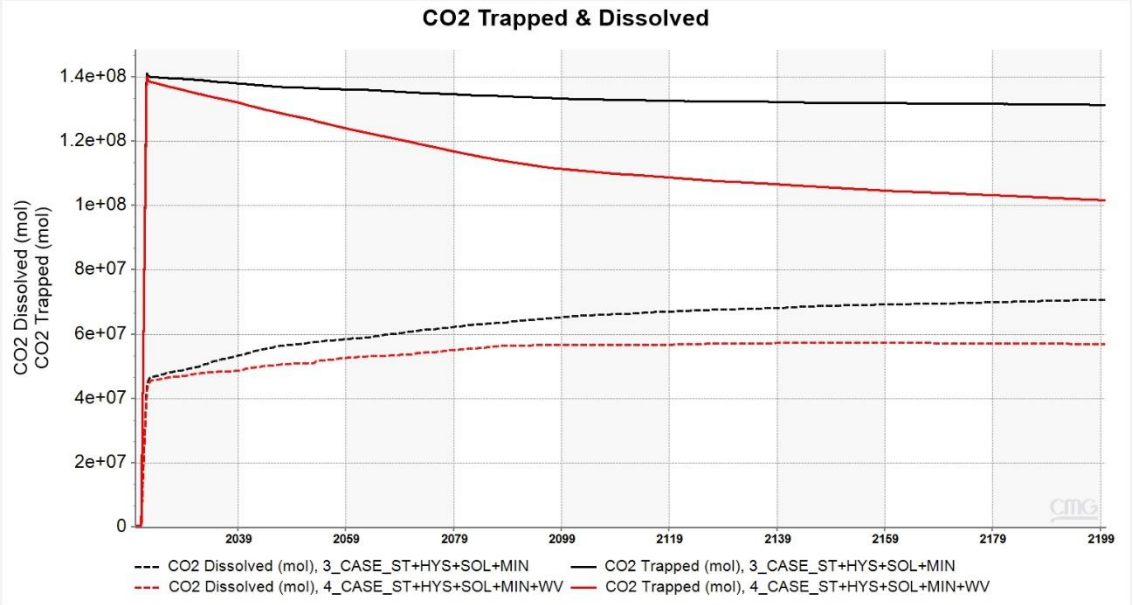

Fig. 29: 4_Case: CO_2 trapped, dissolved, and comparison with 3_Case.

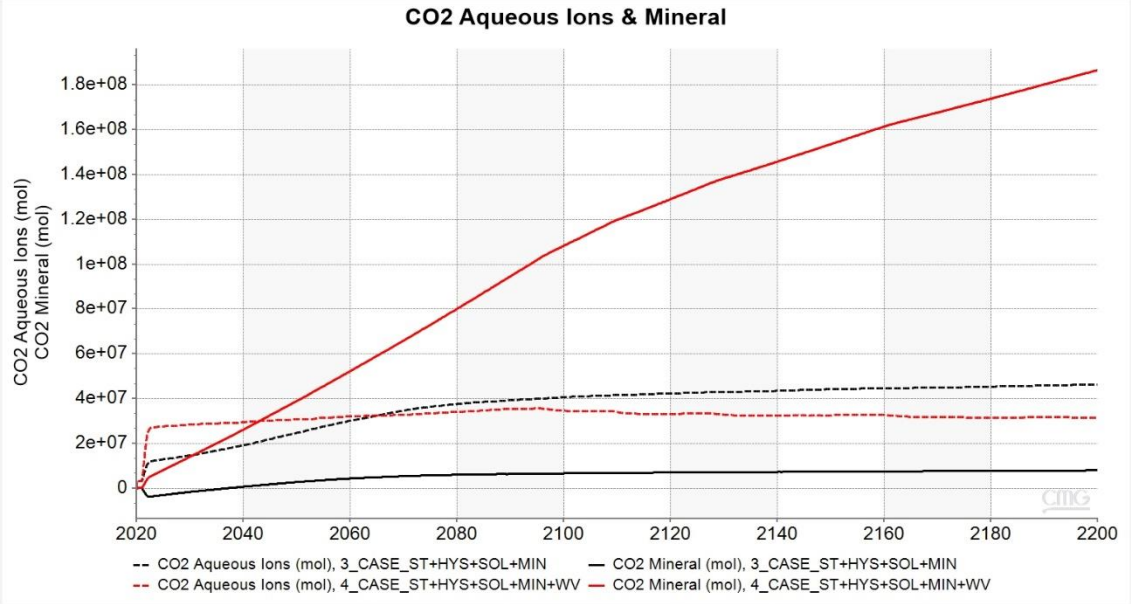

Fig. 30: 4_Case: CO_2 aqueous ions, mineral, and comparison with 3_Case.

In spite of the smaller amounts of CO_2 trapped by almost all trapping mechanisms as reported in figures 29 and 30, a remarkable increase in the amount of CO_2 trapped as a mineral is observed in the fourth case. In detail, the amount of CO_2 mineralized went up from 349.000 kg in the third case to 8.216.000 kg in case four, with a 2350% increase.

4_Case	Total CO_2 Injected	51.112.000 kg	Trapped % of total CO_2
	Capillary trapping		
	+ hysteresis	4.476.000 kg	8.7
	Dissolved in water	2.503.000 kg	4.9
	Aqueous Ions	1.386.000 kg	2.7
	Mineral Precipitate	8.216.000 kg	16
	Total CO_2 trapped	16.581.000 kg	**32.3**

Table 15: 4_Case: % of total CO_2 injected trapped.

The effect of water vaporization in the fourth case accounts for an additional 10.4% of the injected CO_2 compared to the third case.

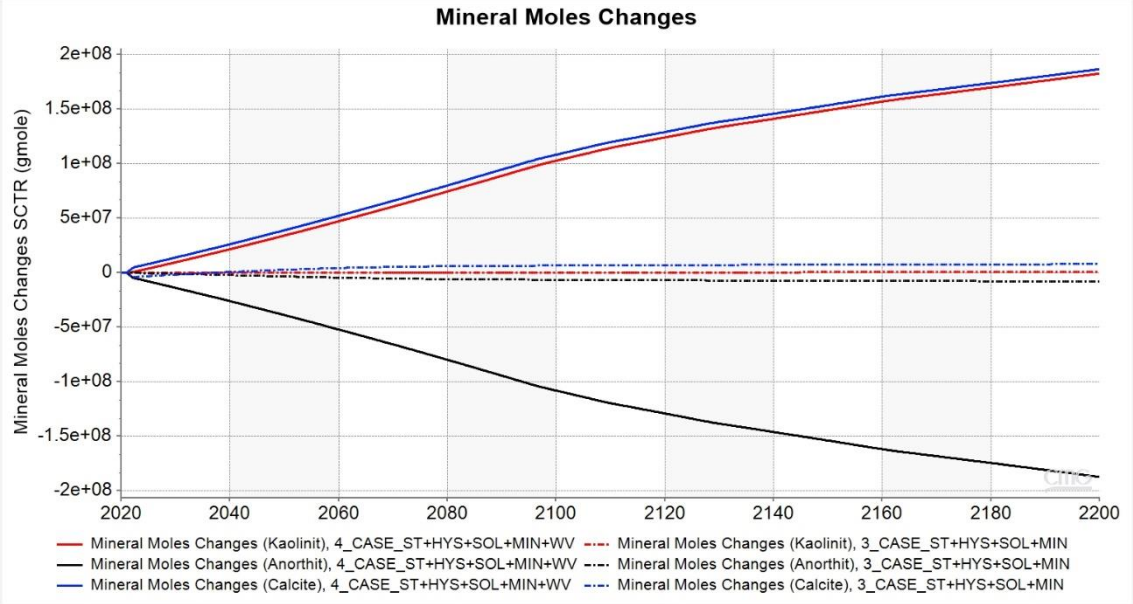

Fig. 31: 4_Case: Mineral mole changes and comparison with 3_Case.

Even if the 180 years are considered short to observe significant amounts of CO_2 becoming mineralized, by looking at the above figure, the vast changes in mineral moles due to water vaporization are distinguished.

In figures 32, 33 and 34, the effect of water vaporization and the mineral mole changes of Anorthite, Kaolinite, and Calcite are visualized.

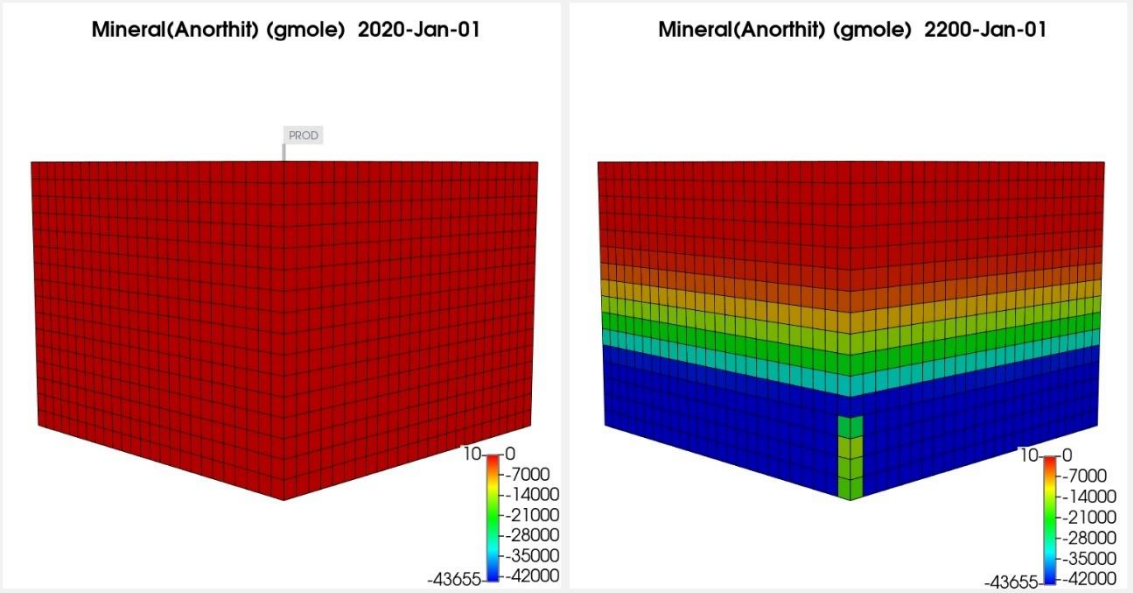

Fig. 32: 4_Case: Mineral mole changes (Anorthite).

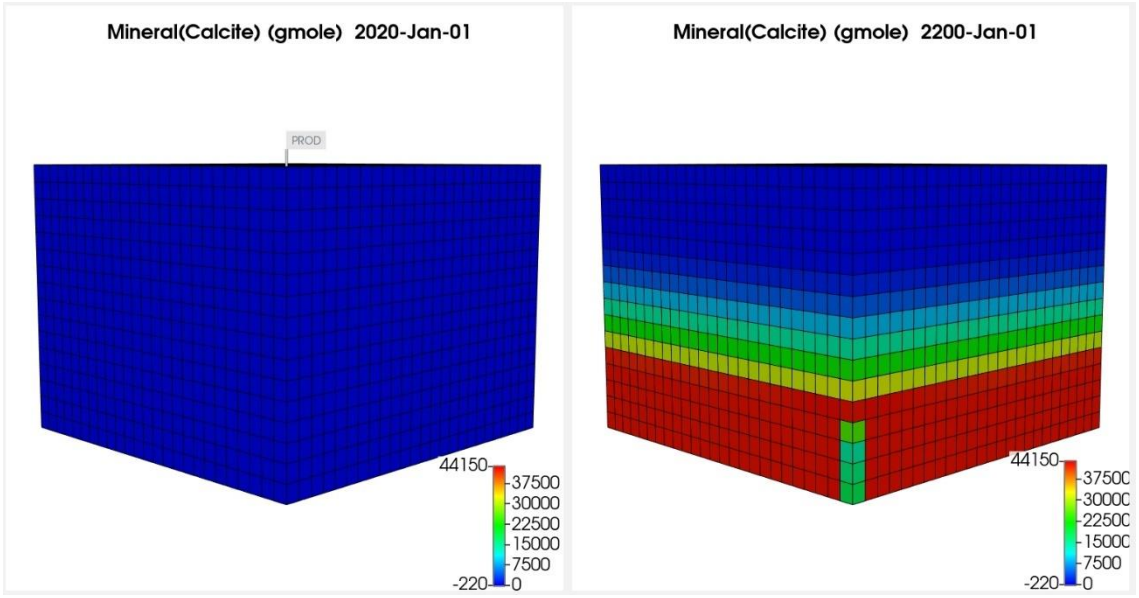

Fig. 33: 4_Case: Mineral mole changes (Calcite).

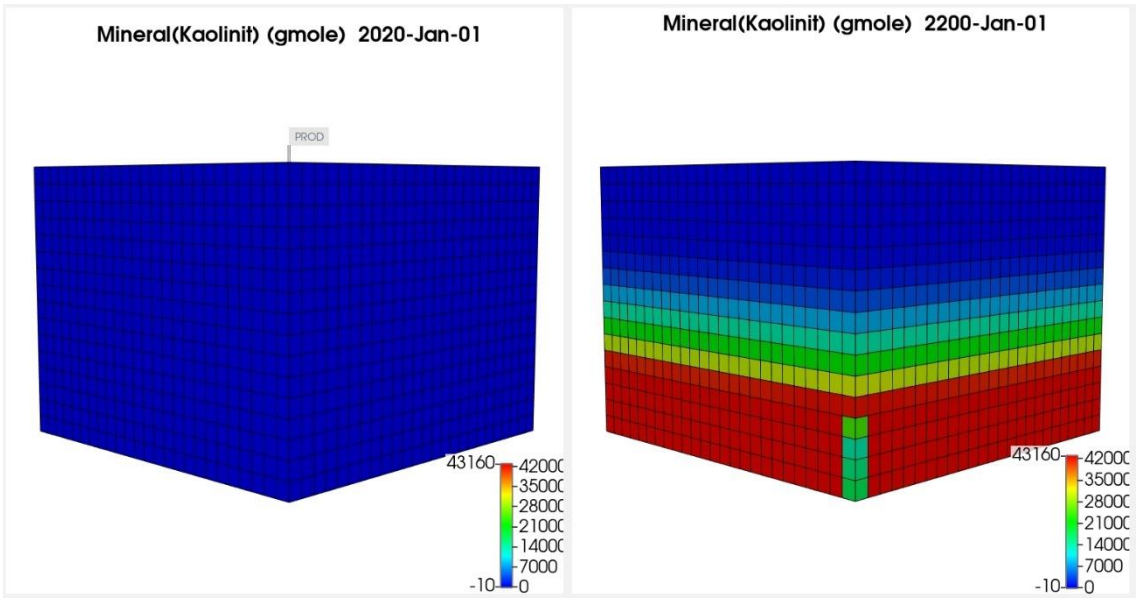

Fig. 34: 4_Case: Mineral mole changes (Kaolinite).

As predicted, just like in the third case, mineral mole changes primarily occur in the bottom layers. However, it is clear that the mineralization changes are now far more distinct between the layers. Furthermore, the effect of water vaporization is observed only in the blocks where perforations were located.

6.4.4.2 1000-year simulation

Due to the significant effect water vaporization seems to have on the amount of CO_2 trapped as minerals precipitate, it was decided to run the simulation of the fourth case for 1000 years instead of 180, up to the date 01-01-3000.

Figure 35 shows that the declining trend of the bottom hole pressure is maintained as more CO_2 is mineralized. By looking at figures 36 and 37, it is apparent that CO_2 mineralization features a significant increase throughout the 1000-year period, whereas, the free, dissolved and residual CO_2 feature a gradual and slow decrease.

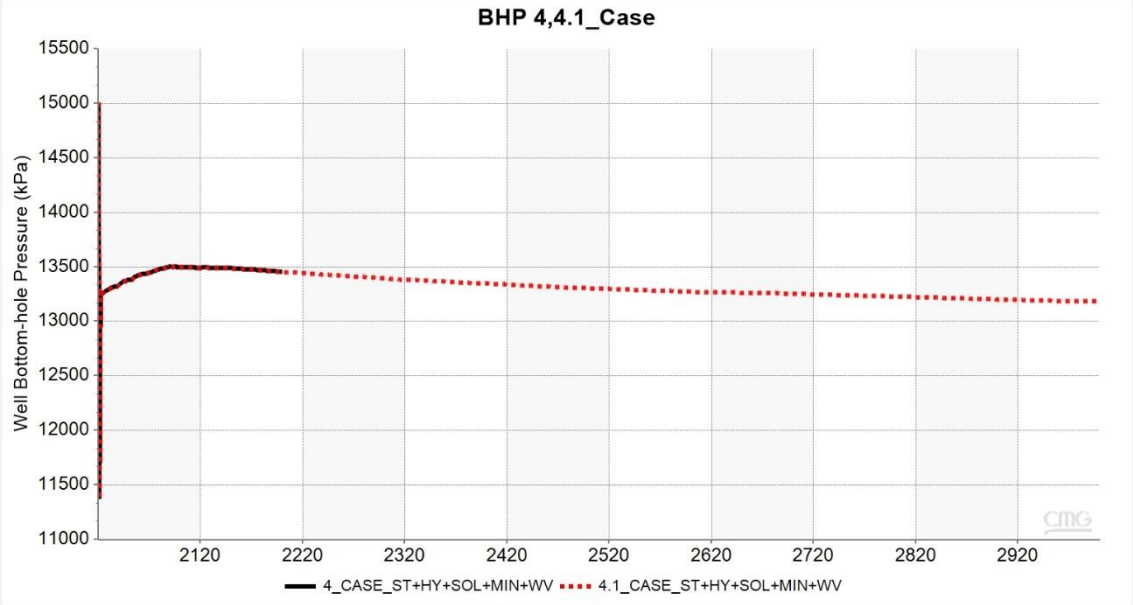

Fig. 35: 4.1_Case: Bottom hole pressure (BHP).

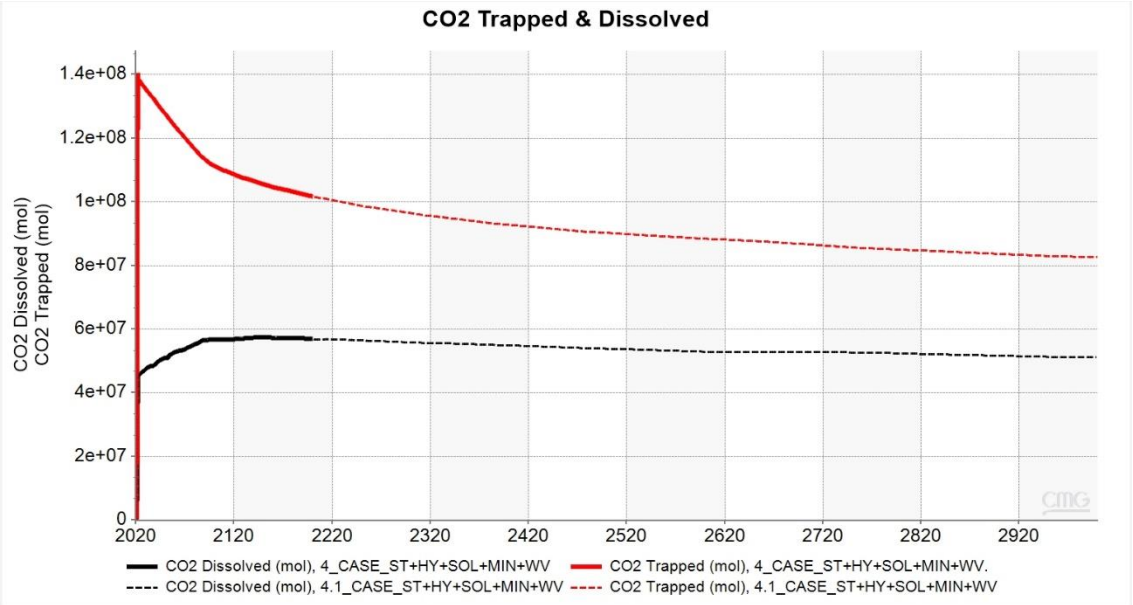

Fig. 36: 4.1_Case: CO_2 trapped, dissolved, and comparison with 4_Case.

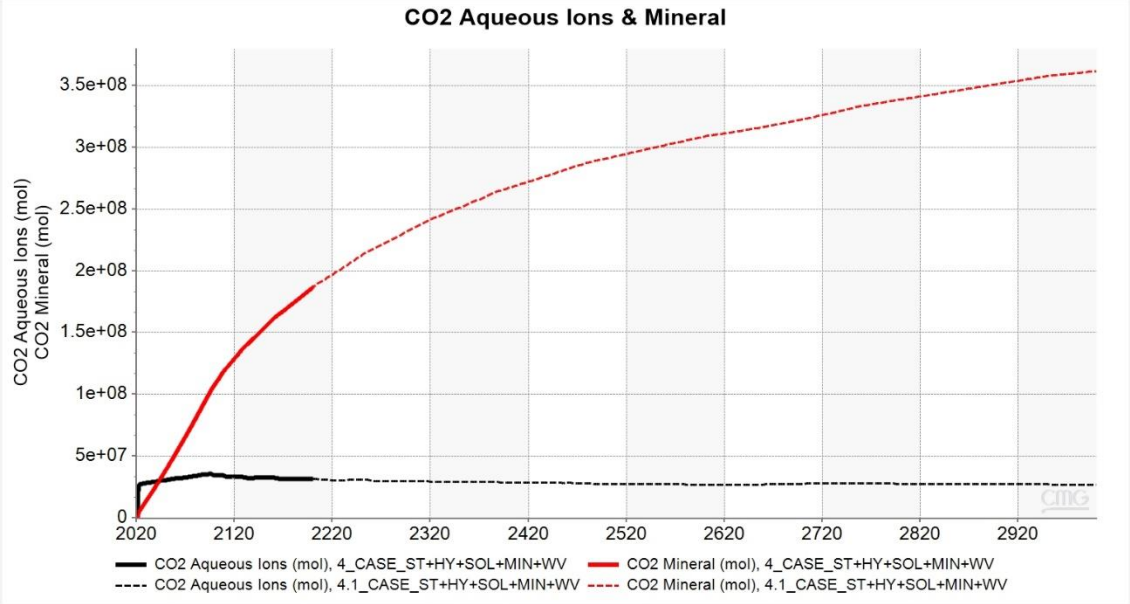

Fig. 37: 4.1_Case: CO_2 aqueous ions, mineralized, and comparison with 4_Case.

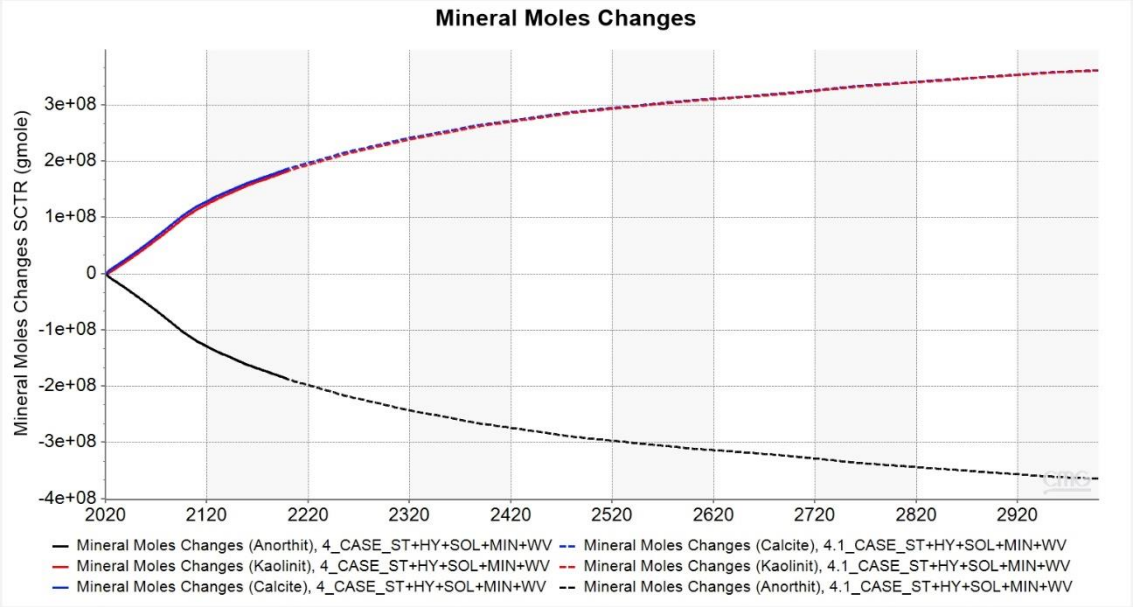

Fig. 38: 4.1_Case: Mineral mole changes and comparison with 4_Case.

The trend of the mineral mole changes is maintained constant between the 180-year and the 1000-year case, proving that calcite and kaolinite continue to precipitate over time, while anorthite dissolves.

Specifically, the amount of CO_2 in mineral form goes up from 8.216.000 kg in 2200, in the fourth case, to 15.921.000 kg in 3000, in the 1000-year case. This indicates, that extending the duration of the simulation could even further increase the amount of mineral precipitate.

All in all, extending the duration of the simulation to 1000 years, accounts for an additional 12.4% trapped of the injected CO_2.

4.1_Case	Total CO_2 Injected	51.112.000 kg	Trapped % of total CO_2
	Capillary trapping		
	+ hysteresis	3.634.000 kg	7.1
	Dissolved in water	2.248.000 kg	4.4
	Aqueous Ions	1.173.000 kg	2.3
	Mineral Precipitate	15.921.000 kg	31
	Total CO_2 trapped	22.976.000 kg	**44.8**

Table 16: 4.1_Case: % of total CO_2 injected trapped.

The impact of water vaporization on CO_2 mineralization, along with the mineral mole changes for the three minerals of the reservoir are depicted in figures 39 and 40, for timesteps 01-01-2500 and 01-01-3000. Mineralization continues to occur in the rock volume, together with the dispersion of the CO_2 in the reservoir as it progressively rises to the top of the reservoir.

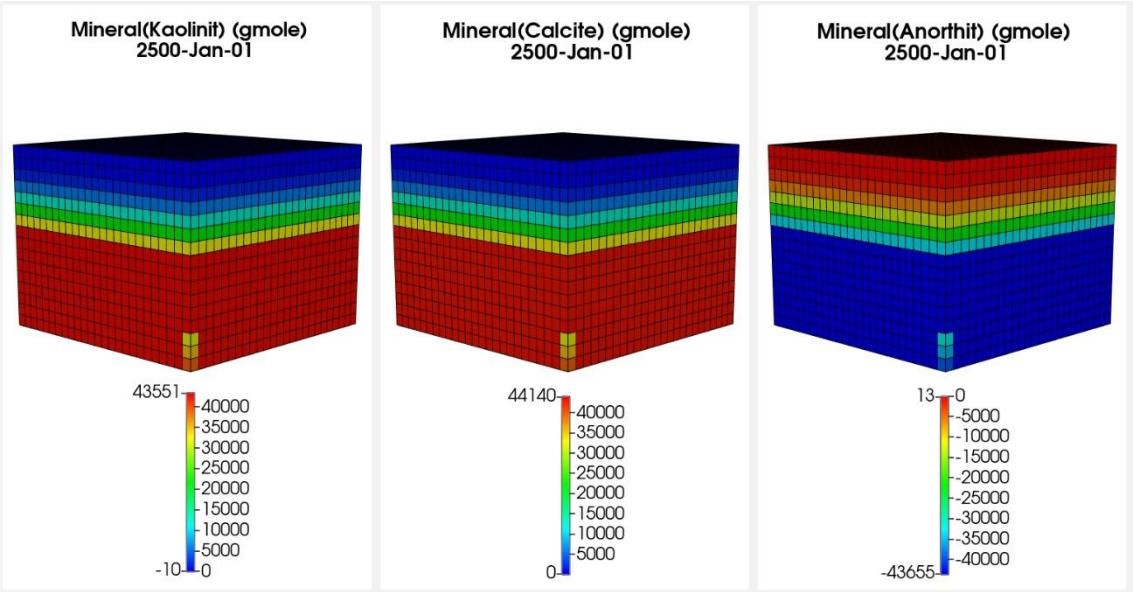

Fig. 39: 4.1_Case: All mineral mole changes (2500).

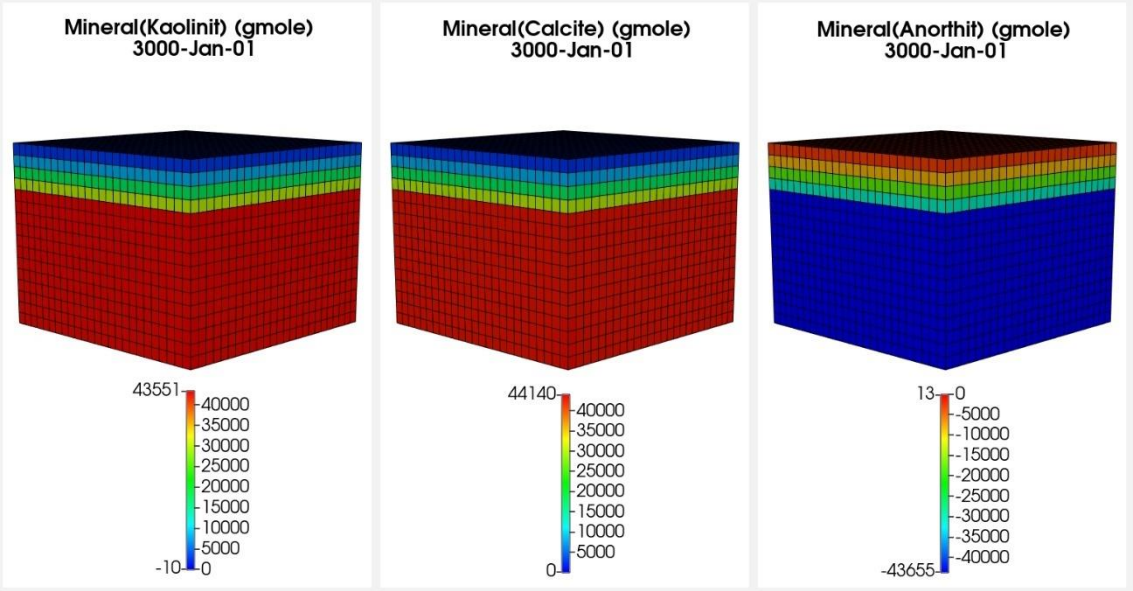

Fig. 40: 4.1_Case: All mineral mole changes (3000).

6.5 Scenario 2: presentation of simulation results

Another gas production-injection scenario was tested to simulate reservoir depletion, and to analyze the effect of production history. In this scenario, the reservoir pressure approaches the initial pressure Parameters such as the reservoir's physical and rock-fluid properties, fluid model, and well properties remained unchanged.

In this scenario, the base model (6_Case) already incorporates solubility and hysteresis trapping on top of structural trapping. The other trapping mechanisms are added one at a time to see how each process affects CO_2 distribution as a free fluid, as a trapped fluid, and as a mineral over time.

In fig. 41 and table 17, the amounts of total injected CO_2 for the two production-injection are reported.

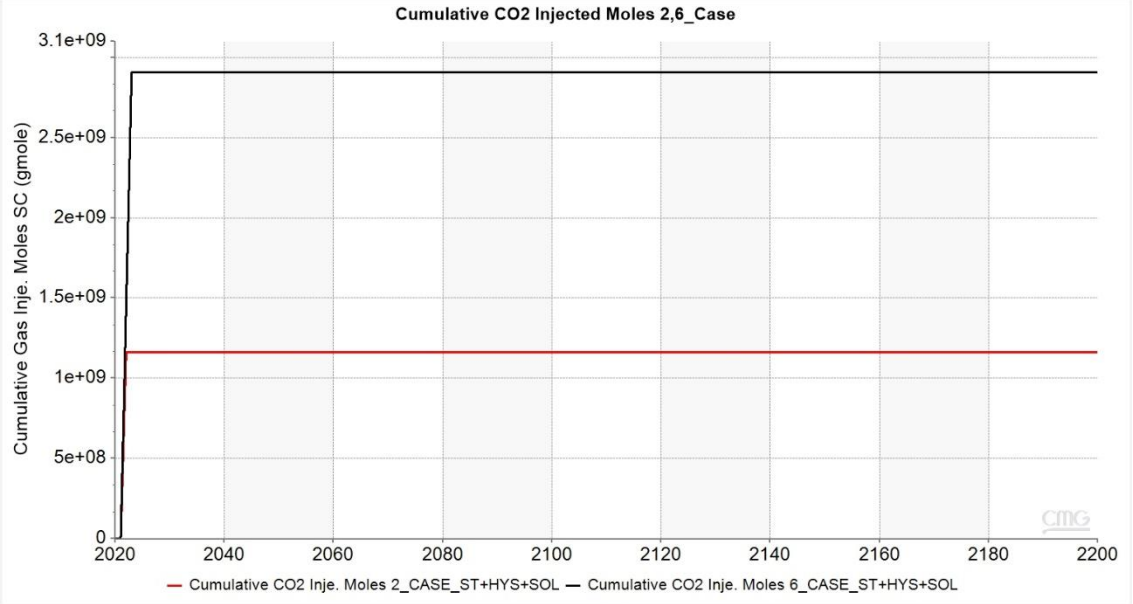

Fig. 41: 6_Case: Comparison of the total CO_2 injected between the two scenarios.

Production-Injection scenario	Total CO_2 Injected
2_Case (Scenario 1)	51.112.000 kg
6_Case (Scenario 1)	76.785.000 kg

Table 17: CO_2 amounts injected in the two scenarios.

Because of the 25% increase in the injection rate, the increase in CO_2 mass injected in the reservoir amounts to 33.5%.

6.5.1 Base model with structural trapping, solubility and capillary trapping

Exactly like in the second case of the first scenario, the effect of the maximum residual gas saturation was evaluated by using two different values, the software's default value, and equal to the critical gas saturation of the In-Salah field. Additionally, the solubility was the same modified version of the Henry's constant model with improvements based on ENI experimental data.

6.5.1.1 Default value for maximum residual gas saturation

First, the software's default value for maximum residual gas saturation was used.

The effect that the additional injected CO_2 had on bottom hole pressure can be viewed in figure 42.

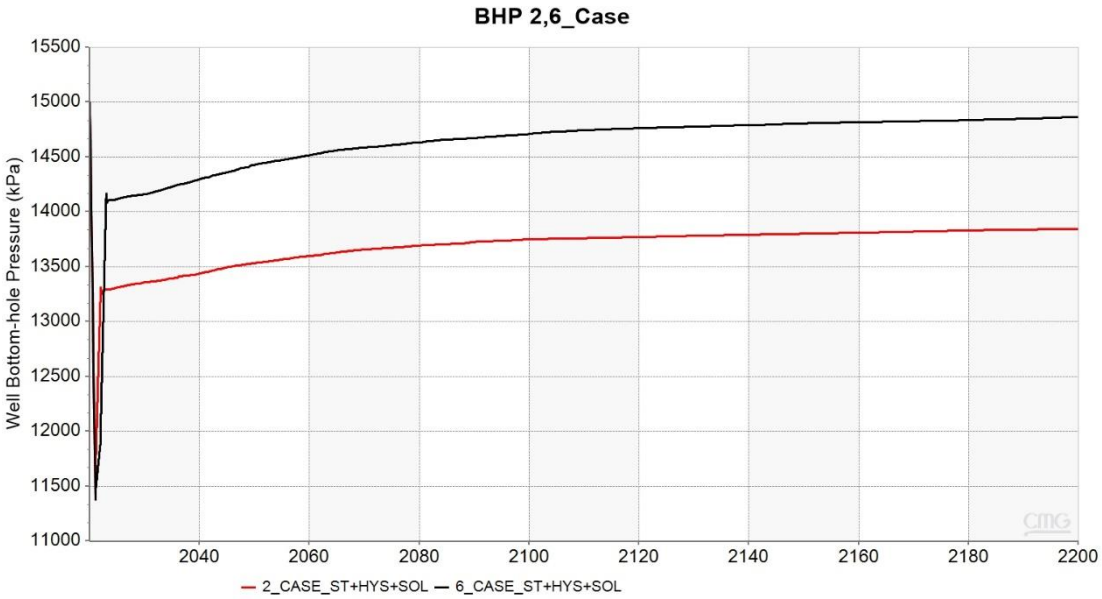

Fig. 42: 6_Case: Bottom hole pressure (BHP) and comparison with 2_Case.

Despite the two-year production in the second scenario, the pressure drop is similar, with the lowest pressure recorded at around 11,300 kPa or 113 bar. Nevertheless, in the second scenario, the reservoir's pressure after injection stabilizes at a sizable plus 10 bar difference (14,800 kPa), almost reaching the initial pressure (15,000 kPa).

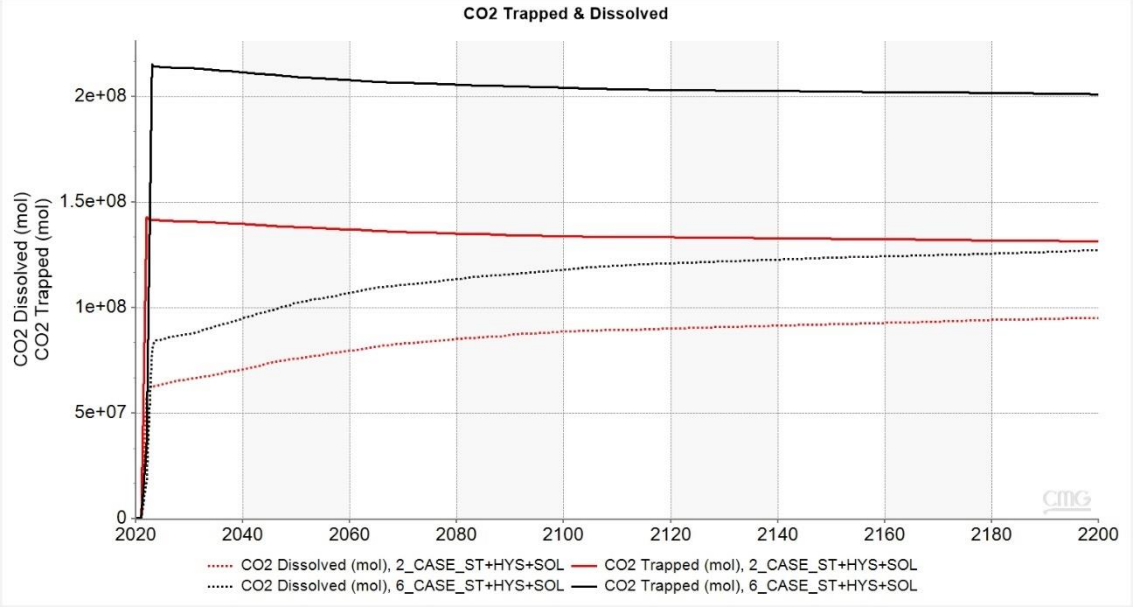

Fig. 43: 6_Case: CO2 trapped, dissolved, and comparison with 2_Case.

6_Case	Total CO_2 Injected	76.785.000 kg	Trapped % of total CO_2
	Capillary trapping		
	+ hysteresis	8.847.000 kg	11.5
	Dissolved in water	5.600.000 kg	7.3
	Total CO_2 trapped	14.447.000 kg	**18.8**

Table 18: 6_Case: % of total injected CO_2 trapped.

Despite the fact that each mechanism in the second scenario traps more CO_2, the percentage of total trapped CO_2 is lower than in the first scenario. In detail, 19.5 percent of total CO_2 was trapped in the second case of the first scenario (2_Case), whereas 18.8 percent was trapped in this case.

6.5.1.2 Maximum residual gas saturation equal to In Salah's field critical gas saturation

Second, the value of maximum residual gas saturation, was set equal to the critical gas saturation of the In-Salah field.

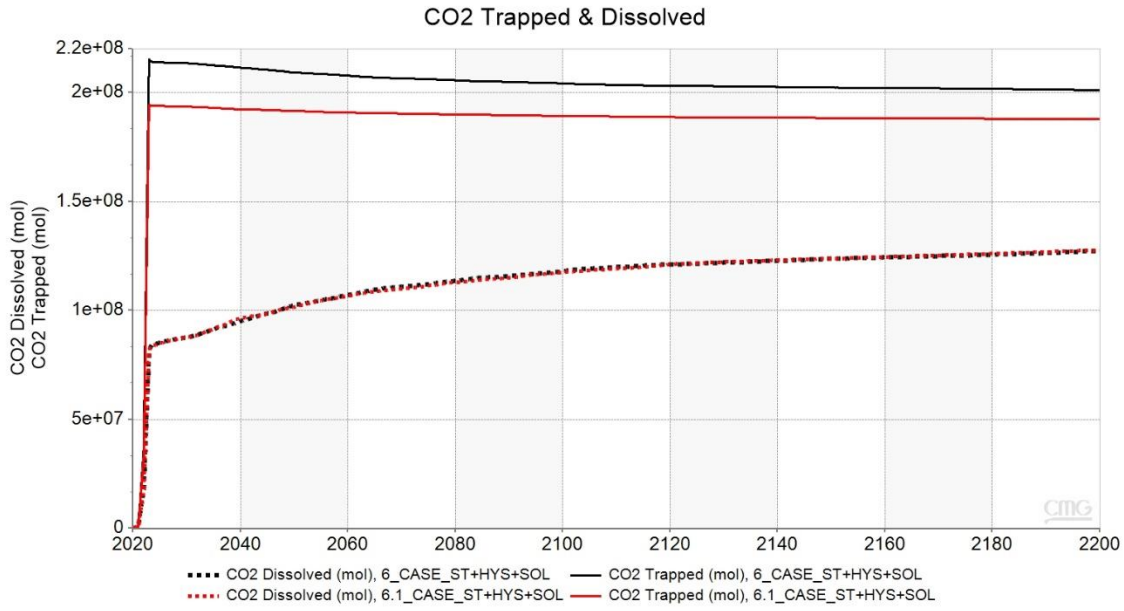

Fig. 44: 6.1_Case: CO_2 trapped, dissolved and comparison with 6_Case.

As expected, there is no variation to the volume of CO_2 dissolved between the two cases (6 and 6.1), since the solubility model was not changed. Although, the amount of

trapped CO_2 through structural and hysteresis trapping is lower in this case with the lower value for maximum residual gas saturation.

6.1_Case	Total CO_2 Injected	76.785.000 kg	Trapped % of total CO_2
	Capillary trapping + hysteresis	8.260.000 kg	10.8
	Dissolved in water	5.612.000 kg	7.3
	Total CO_2 trapped	13.872.000 kg	**18.1**

Table 19: 6.1_Case: % of total injected CO_2 trapped.

Again, between the corresponding cases of the two scenarios, cases 2.1 and 6.1, regardless of the greater amounts trapped by each mechanism, the total CO_2 trapped in the second scenario is 0.7 percent less (18.1%), than in the first scenario (18.8%).

6.5.2 Model with structural trapping, solubility trapping, capillary trapping, and mineral trapping

The next model (7_Case) was then obtained from the previous (6_Case), which incorporates capillary and solubility trapping, by introducing mineralization due to CO_2.

Regarding activity model, aqueous reactions, mineral composition, initial volume fractions, pH, and original species concentrations, the values and model choices were the same as in scenario 1.

As it can be observed, mineralization has a small effect of an approximately - 0.5 bar on the reservoir pressure the at the end of the simulation.

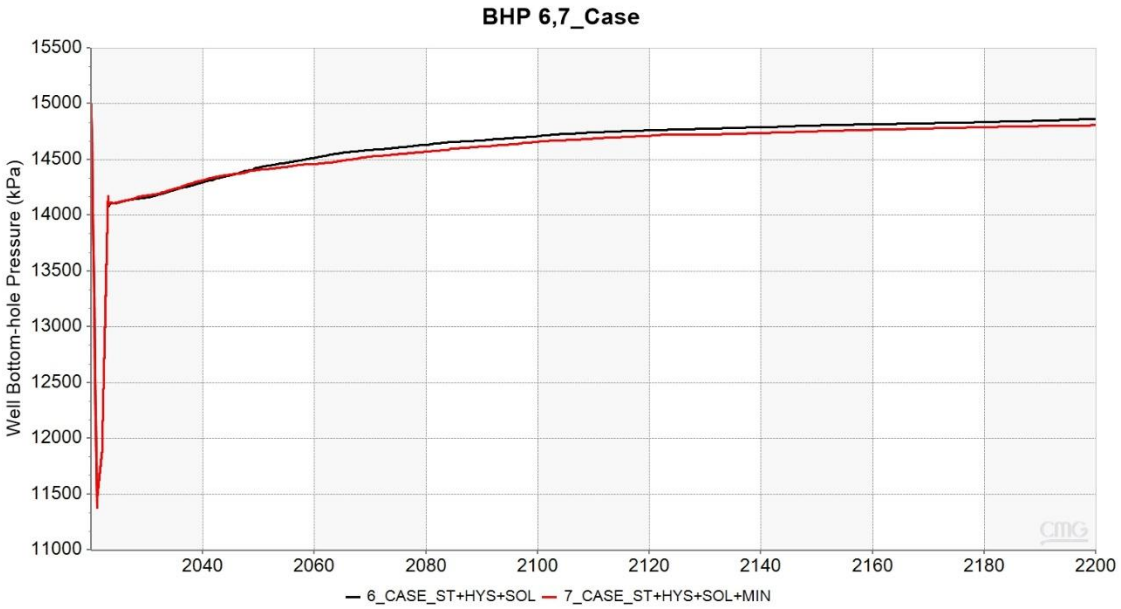

Fig. 45: 7_Case: Bottom hole pressure (BHP).

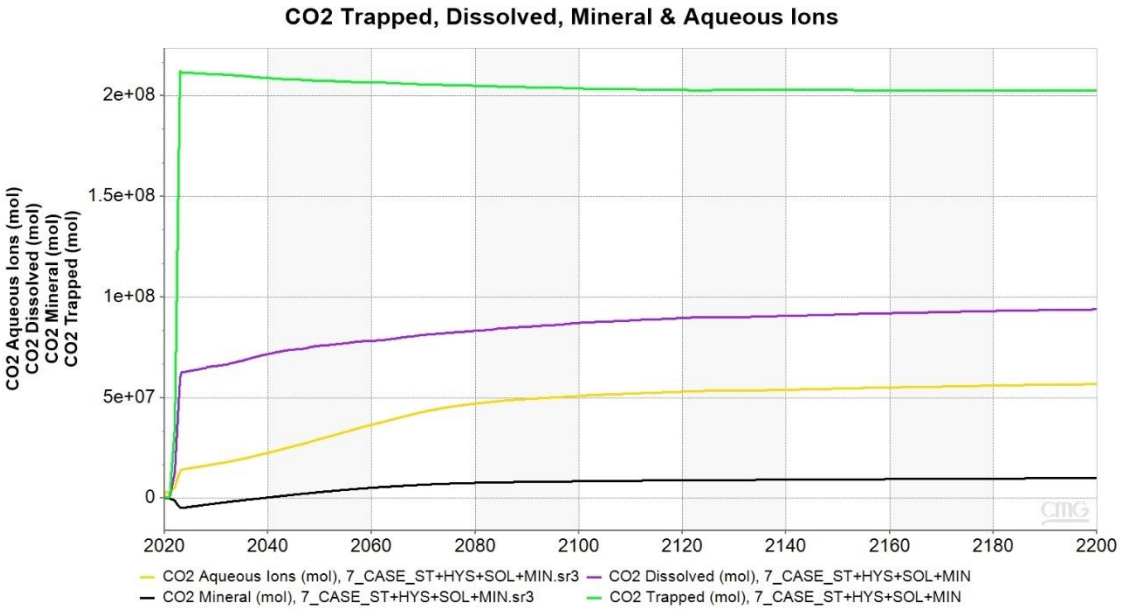

Fig. 46: 7_Case: CO_2 trapped, dissolved, mineral, and aqueous ions.

7_Case	Total CO_2 Injected	76.785.000 kg	Trapped % of total CO_2
	Capillary trapping		
	+ hysteresis	8.926.000 kg	11.6
	Dissolved in water	4.132.000 kg	5.4
	Aqueous Ions	2.498.000 kg	3.2
	Mineral Precipitate	444.000 kg	0.6
	Total CO_2 trapped	16.000.000 kg	**20.8**

Table 20: 7_Case: % of total injected CO_2 trapped.

In this case, the effect of CO_2 mineralization has an even insignificant effect in the amount of CO_2 trapped in mineral form, with less than 1% of the total CO_2 injected, trapped as a mineral precipitate.

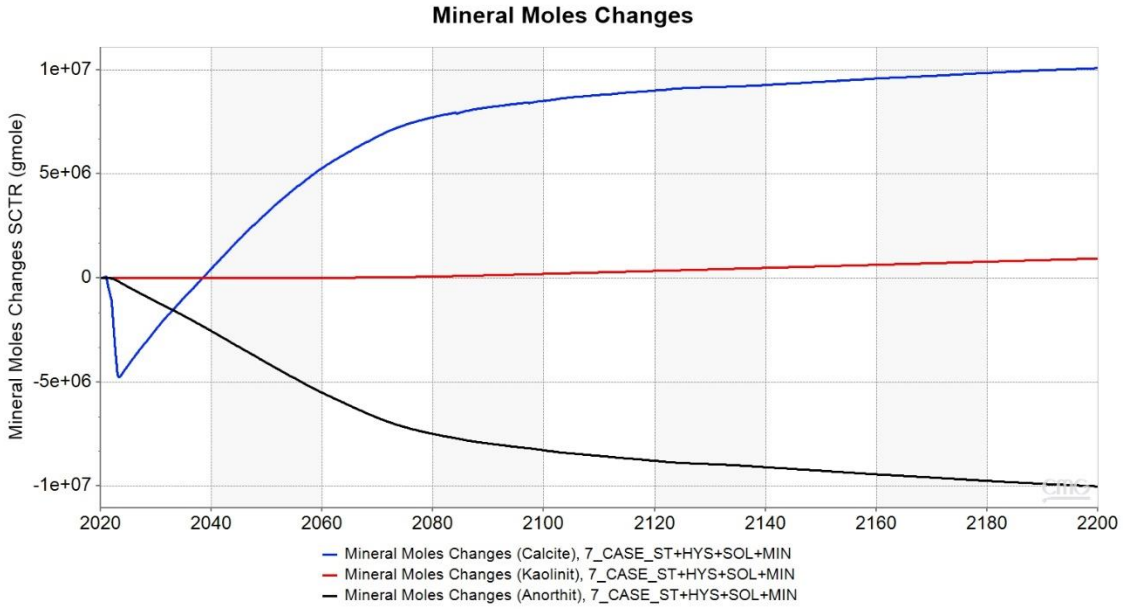

Fig. 47: 7_Case: Mineral mole changes.

In detail, there was an increase 21.4% of 95,000 kg of mineral precipitate between the corresponding cases of the two injection scenarios, but still, half of the total CO_2 in the reservoir, is trapped due to structural and capillary trapping.

6.5.3 Model with structural trapping, solubility trapping, capillary trapping, mineral trapping, and water vaporization

Lastly, the process of water vaporization was added to the model of the previous case (7_Case).

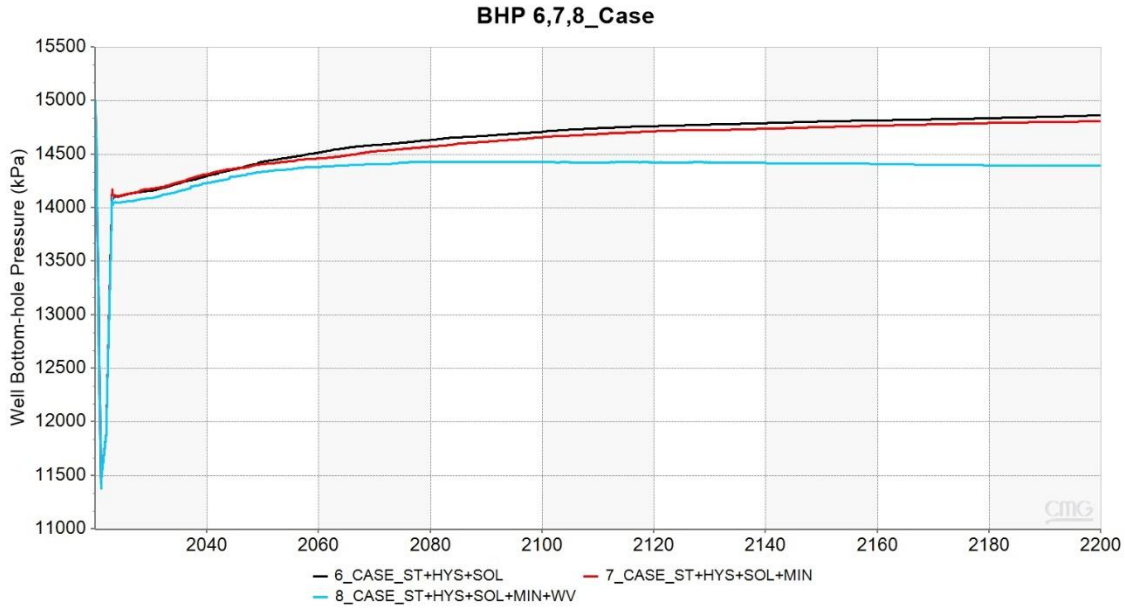

Fig. 48: 8_Case: Bottom hole pressure (BHP).

As in scenario 1, the effect of water vaporization on the bottom hole pressure is evident, causing the reservoir pressure to stabilize at a lower value than in the other cases.

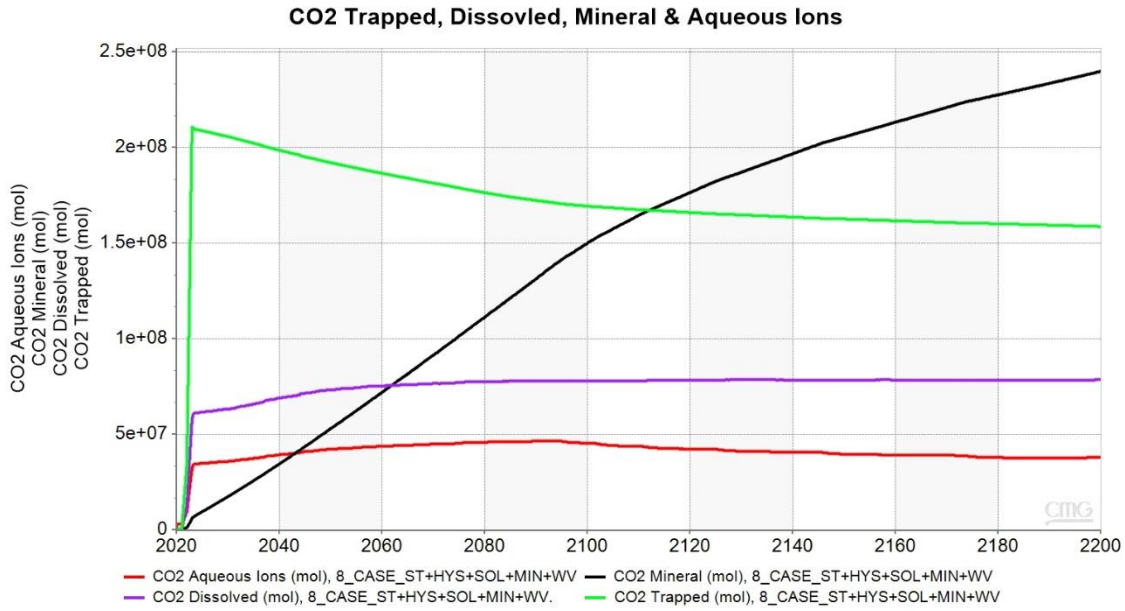

Fig, 49: 8_Case: CO_2 trapped, dissolved, mineral, and aqueous ions.

There is also a considerable increase in the amount of CO_2 trapped as a mineral in case 8, exactly as in case 4.

8_Case	Total CO_2 Injected	76.785.000 kg	Trapped % of total CO_2
	Capillary trapping + hysteresis	6.983.000 kg	9.1
	Dissolved in water	3.456.000 kg	4.5
	Aqueous Ions	1.670.000 kg	2.2
	Mineral Precipitate	10.561.000 kg	13.7
	Total CO_2 trapped	22.670.000 kg	**29.5**

Table 21: 4_Case: % of total CO_2 injected trapped.

Even though percentagewise there is a 13% increase in CO_2 mineral precipitate from case 7 to case 8 due to the process of water vaporization, the percentage of CO_2 trapped by mineral trapping is still less than the percentage of the corresponding case 4 of scenario 1. Not only that, but in spite of the additional 25.673.000 kg of CO_2 in scenario 2, the percentage trapped with respect to the total CO_2 in the reservoir, is less than the corresponding of scenario 1.

6.6 Summary of simulator's results

Simulations presented in this chapter for the two production-injection scenarios included all the trapping mechanisms relevant in carbon storage. Similar results have been obtained between the two scenarios. However, both cases emphasized the importance of considering the geochemical trapping processes, together with the implementation of water vaporization while designing and developing a CO_2 storage project.

Next, an overview of the results obtained is presented in which the trapped amounts of CO_2 are compared between the different trapping mechanisms in the models employed.

6.6.1 Scenario 1

In production-injection scenario 1, 51.112.000 kg of CO_2 were injected. The table below shows the percentages of CO_2 trapped by every mechanism that was progressively

incorporated in all the different models built, as well as the total percentage of CO_2 trapped with respect to the CO_2 injected.

In table 22 are reported, for all cases of scenario 1, the percentages of CO_2 trapped by each individual trapping mechanism, with respect to the injected amount of CO_2. In all cases the rest of the CO_2 remains in the reservoir in supercritical phase, or has not yet been trapped by any of the trapping mechanisms.

	Total mass of CO_2 injected = 51.112.000 kg	**Scenario 1 Cases**					
		1	**2**	**2.1**	**3**	**4**	**4.1**
% of CO_2 trapped by each trapping mechanism with respect to the total CO_2 injected	Structural trapping	88.5	80.5	81.2	78	67.6	55.2
	Capillary trapping	11.5	11.3	10.6	11.0	8.7	7.1
	Solubility trapping		8.2	8.2	6.0	4.9	4.4
	Aqueous Ions				4.0	2.7	2.3
	Mineral trapping				1.0	16	31
	Total	**100**					

Table 22: Scenario 1: Percent of CO_2 trapped by each trapping mechanism with respect to the total mass of CO_2 injected, for all cases.

Overall, a significant increase to the total amount of CO_2 trapped was observed as more trapping mechanisms were considered in the models.

An increase close to 8% of the total CO_2 trapped was observed between cases 1, 2, and 2.1 when solubility was implemented. The magnitude of this trapping mechanism seems to lower as more mechanisms are added, or if a longer duration for the simulation was selected, dropping from 8% to 6% in case 3, to 4.9% in case 4, and to 4.4% in case 4.1.

Even though CO_2 is heavier than CH_4, and during injection it accumulates at the bottom layers, a gradual dispersion in the reservoir was observed. Additionally, since this study was focused on the key parameters and trapping mechanisms of carbon storage, the caprock integrity aspect was not investigated. CO_2 migration to the top of the reservoir was hindered by capillary trapping, and the amount of CO_2 trapped by this mechanism is close to 50% of the total amount for cases 2, 2.1 and 3.

When mineralization of CO_2 was first implemented in case 3, compared to cases 2 and 2.1, it did not seem to have a great influence on the total amount of CO_2. Specifically, mineral trapping accounts for just 1% of the total CO_2 trapped, while ionic trapping for an additional 4%. However, when water vaporization was added together with mineralization of CO_2 in case 4, mineral trapping became the prevailing trapping mechanism with almost 50% of the CO_2 trapped in mineral form. In addition, this process

alone led to an increase to the total CO_2 permanently trapped from 22% in case 3, to 32.3% in case 4.

Lastly, the importance of mineral trapping was emphasized in case 4.1 where the duration of the simulation lasted 1000 years; in this case the amount of CO_2 trapped by mineral trapping almost became double, from 16% in case 4, to 31% in case 4. Also, this amount now accounts for close to 70% of the total CO_2 permanently trapped.

6.6.2 Scenario 2

In the second production-injection scenario 2, 76.785.000 kg of CO_2 were injected. Again, the following table summarizes the percentages of CO_2 trapped by each mechanism that was successively added into the model, including the total percentage of CO_2 trapped as a percentage of the CO_2 injected.

In table 23 are reported respectively, for all cases of scenario 2, the percentages of CO_2 trapped by each trapping mechanism, with respect to the injected amount of CO_2. Again, in all cases the rest of the CO_2 remains in the reservoir in supercritical phase, or has not yet been trapped by any of the trapping mechanisms.

	Total mass of CO_2 injected = 76.785.000 kg	**Scenario 2 Cases**			
		6	**6.1**	**7**	**8**
% of CO_2 trapped by each trapping mechanism with respect ot the total CO_2 injected	Structural trapping	81.2	81.9	79.2	70.5
	Capillary trapping	11.5	10.8	11.6	9.1
	Solubility trapping	7.3	7.3	5.4	4.5
	Aqueous Ions			3.2	2.2
	Mineral trapping			0.6	13.7
	Total	**100**			

Table 23: Scenario 2: Percent of CO_2 trapped by each trapping mechanism, with respect to the total mass of CO_2 injected, for all cases.

Similar results have been obtained between scenario 2, and scenario 1 with respect to the total amount of CO_2 trapped, once again emphasizing the importance of including the process of water vaporization together with mineral trapping.

Nevertheless, it was expected that due to the significantly larger amount of injected CO_2, each trapping mechanism would contribute more to the total CO_2 trapped. But, an inversely proportional relationship was observed between the available-injected CO_2, and the amount trapped by every trapping mechanism.

CHAPTER 7

CONLCLUSION AND SUGGESTIONS FOR FUTURE WORK

7.1 Conclusions

Carbon storage is a method for reducing greenhouse gas emissions. The primary issues are the long-term CO_2 containment and costs.

The objective of this research was to investigate how critical it is to model, the physical and chemical CO_2 trapping mechanisms that occur in a depleted gas reservoir, where CO_2 is injected for geological storage in order to predict and quantify the amount of CO2 which becomes permanently trapped. This was accomplished through the use of a commercial software specifically designed to predict CO_2 flow and geochemical reactions in the formations.

Following the assumption of a simplified reservoir geometry and the generation of the reference model, two gas production scenarios were simulated to mimic reservoir depletion under pressure and temperature conditions so that CO_2 remained in the supercritical phase in the reservoir. In total, 10 different models were built and simulated, with the initial simulations only including structural trapping, while the other trapping mechanisms were progressively added.

The results primarily emphasized the importance of considering geochemical trapping processes while designing and developing a CO_2 storage. Second, mineral trapping seems to be significantly influenced by the process of water vaporization. When water vaporization was modeled, a major increase in mineral precipitate was seen, which is a benefit because mineral trapping is regarded the safest trapping mechanism.

Next, accurate modelling of CO_2 solubility in brine is important because of the substantial amounts of trapped CO_2 in brine. CO_2 solubility in brine is a function of temperature, pressure and salinity, and by comparing 3 available models (also implemented in the software), it was seen that even though the temperature was constant and uniform, the solubility varied between the models.

As a result, accurate laboratory experiments to define mineralogy and brine are particularly relevant to fully characterize the system.

Moreover, relative permeability hysteresis has been shown to have a significant influence on CO_2 inventory, and is thus regarded as one of the crucial information to be identified.

The software's main limitation was the inability to model solubility and hysteresis trapping separately. Both processes had to be modelled simultaneously.

The approach taken in this research can be used as a guideline to identify the key parameters impacting on CO_2 trapping for a given reservoir, and aspects that need to be taken into consideration while designing a CO_2 storage project.

7.2 Suggestions for future work

The models employed in this research were developed to assess the trapping potential of all trapping mechanisms taking place in a CO_2 storage

A simplification was assumed in the composition of the reservoirs' gas, being only methane, and mostly it was assumed that pure CO_2 was injected. Impurities' influence on CO_2 are seldom researched, and further research is required to determine their impact on geochemical processes.

For the models to be credible, they must be based on solid data. Absence of geological, and rock-fluid data are the major drawbacks of geochemical modeling.

REFERENCES

1) Keeling, C. D. and Whorf, T. P.: Atmospheric Carbon Dioxide Record from Mauna Loa.

2) International Energy Outlook 2007; Energy Information Administration, US Department of Energy (EIA): Washington, DC, USA, May 2007.

3) United Nations Framework Convention on Climate Change (UNFCCC), 2015, Adoption of the Paris Agreement, 21st Conference of the Parties, Paris, France.

4) Climate Change 2001, UN Intergovernmental Panel on Climate Change (IPCC) Third Assessment Report.

5) United Nations Framework Convention on Climate Change (UNFCCC), Kyoto Protocol Reference Manuel on Accounting of Emissions and Assigned Amounts, 2008.

6) IPCC, 2005, IPCC Special Report on Carbon Dioxide Capture and Storage, Cambridge University Press, Cambridge, United Kingdom, New York, NY, USA.

7) Bachu, S., Gunter, WD. and Perkins, EH: "Carbon Dioxide Disposal," Aquifer Disposal of Carbon Dioxide, Brian Hitchon Editor, Geoscience Publishing Ltd, 1996, 11-22.

8) Hitchon, B., Gunter, WD., Gentziz, T. and Bailey, RT "Sedimentary Basins and Greenhouse Gases: A Serendipitous Association," Energy Convers. Mgmt., Vol. 40 (1999) 825-843.

9) Carbon Sequestration Technology Roadmap and Program Plan; United States Department of Energy/Office of Fossil Energy/National Energy Technology Laboratory (USDOE/FE/NETL): Pittsburgh, PA, USA, 2007.

10) International Panel on Climate Change (IPCC). IPCC Special Report on Carbon Dioxide Capture and Storage; Metz, B., Davidson, O., de Coninck, H., Loos, M., Meyer, L., Eds.; Cambridge University Press: Cambridge, UK, 2005; p. 195.

11) Best Practices for: Monitoring, Verification, and Accounting of CO_2 Stored in Deep Geologic Formation; DOE/NETL-311/081508; United States Department of Energy/Office of Fossil Energy/National Energy Technology Laboratory, Pittsburgh, PA, USA, 2009.

12) Using the Class V Experimental Technology Well Classification for Pilot GS Projects; UIC Program Guidance (UICPG #83); Environmental Protection Agency (EPA): Washington, DC, USA, 2007.

13) Core Energy, LLC Class V UIC Injection Permit; Permit No. MI-137-5X25-0001; Environmental Protection Agency (EPA): Washington, DC, USA, draft version issued July 2008.

14) Underground Injection Control Program (UIC); Environmental Protection Agency (EPA): Washington, DC, USA, 12 February 2008.

15) Geologic Sequestration of Carbon Dioxide; Environmental Protection Agency (EPA): Washington, DC, USA, 2008.

16) Cook PJ (2006) Site characterization. In: International Symposium on Site Characterization for CO_2 Storage, 20–22 March 2006, Berkeley, CA, Lawrence Berkeley National Laboratory, 3–5.

17) Bachu S. (2003) Screening and ranking of sedimentary basins for sequestration of CO_2 in geological media. Environ. Geol., 44(3), 277–289.

18) Benson S and Cook P et al. (2005) Transport of CO_2. In: Metz B, Davidson O, de Coninck H, Loos M and Meyer L (eds), IPCC Special Report on Carbon Dioxide Capture and Storage, Cambridge, UK, Cambridge University Press, 197–276.

19) Gunter W D, Perkins E H and McCann T J (1993) Aquifer disposal of CO_2 -rich gases reaction design for added capacity, Energy Conversion and Management, 34, 941–948.

20) Holtz M and Bryant S (2005) Effects of pore network geometry on permanent storage of sequestered CO_2, AAPG's 2005 Annual Meeting, 19–22 June, Calgary, AB, Canada.

21) Holtz M H, Doughty C, Yeh J and Hovorka S (2004) Modelling of CO_2 saline aquifer sequestration and the effects of residual phase saturation, AAPG Annual Convention, 16–21 April, Dallas, TX.

22) Bertier P, Swennen R, Laenen B, Lagrou D and Dreesen R (2006) Experimental identification of CO_2 –water–rock interactions caused by sequestration of CO2 in Westphalian and Buntsandstein sandstones of the Campine Basin (NE -Belgium), Journal of Geochemical Exploration, 89, 10–14.

23) Gibson-Poole CM, Svendsen L, Underschultz J, Watson MN, Ennis-King J, van Ruth PJ, Nelson EJ, Daniel RF and Cinar Y (2008) Site characterization of a basin-scale CO_2 geological storage system: Gippsland Basin, southeast Australia. Environ. Geol., 54(8), 1583–1606.

24) Bachu S, Bonijoly D, Bradshaw J, Burruss R, Holloway S, Christensen NP and Mathiassen OP (2007) CO_2 storage capacity estimation: Methodology and gaps. Int. J. Greenhouse Gas Control, 1(4), 430–443.

25) Koide H, Tazaki Y, Noguchi Y, Nakayama S, Iijima M, Ito K and Shindo Y (1992) Subterranean containment and long-term storage of carbon dioxide in unused aquifers and in depleted natural gas reservoirs, in Blok K, Turkenburg W, Hendriks C and Steinberg M (eds), Energy Conversion and Management, 33(5–8), 619–626.

26) Dooley J J, Dahowski R T, Davidson C L, Wise M A, Gupta N, Kim S H and Malone EL (2006): Carbon Dioxide Capture and Geologic Storage, a technology report from the second phase of the global energy technology strategy program, Battelle, Joint Global Change Research Institute.

27) USDOE (U.S. Department of Energy, Office of Fossil Energy), 2007. Carbon Sequestration Atlas of United States and Canada.

28) Jakobsen, V. E., Hauge, F., Holm, M. and Kristiansen, B.: CO_2 for EOR on the Norwegian Shelf- a Case Study, Bellona Report, August 2005.

29) Korbfl, R. and Kaddour, A.: Sleipner Vest CO_2 Disposal - Injection of Removed CO_2 into the Utsira Formation, Energy Conversion Management, 36(6-9), 509-512, 1995.

30) Torp, T. A. and Gale, J.: Demonstrating Storage of CO_2 in Geological Reservoirs: The Sleipner and SACS projects, Greenhouse Gas Control Technologies, I, Elsevier, Amsterdam, 311-316, 2003.

31) Gale, J.: Geological Storage of CO_2: What's known, where are the gaps, and what more needs to be done? Greenhouse Gas Control Technologies, I, Elsevier, Amsterdam, 201-206, 2003.

32) https://en.wikipedia.org/wiki/Carbon_dioxide

33) Ennis-King, J. and Paterson, L.: Engineering Aspects of Geological Sequestration of Carbon Dioxide, SPE 77809, Proceedings of the Asia Pacific Oil and Gas Conference and Exhibition, Melbourne, Australia, 8-10 October, 2002.

34) Spycher N, Pruess K and Ennis-King J (2003) CO_2 –H_2O mixtures in the geological sequestration of CO_2. I. Assessment and calculation of mutual solubilities from 12 to 100 °C and up to 600 bar, Geochimica et Cosmochimica Acta, 67, 3015–3031.

35) Carbon Capture and Storage, Parliamentary Office of Science and Technology, post note March 2005, Number: 238.

36) Ran, Q. PhD thesis: Simulation of Geological Carbon Dioxide Storage, Imperial College, London, 2008.

37) Ennis-King, J. and Paterson, L.: Engineering Aspects of Geological Sequestration of Carbon Dioxide, SPE 77809, Proceedings of the Asia Pacific Oil and Gas Conference and Exhibition, Melbourne, Australia, 8-10 October, 2002.

38) Sahni, A., Burger, J. and Blunt, M. J.: Measurement of Three Phase Relative Permeability during Gravity Drainage using CT Scanning. SPE 39655, Proceedings of the SPE/DOE Improved Oil Recovery Symposium, Tulsa, Oklahoma, 19-22 April, 1998.

39) Spiteri, E., Juanes, R., Blunt, M. J. and Orr Jr, F. M.: Relative Permeability Hysteresis: Trapping Models and Application to Geological CO_2 Sequestration, SPE 96448, Proceedings of the SPE Annual Technical Conference and Exhibition, Dallas, Texas, 9-12 October, 2005.

40) Dong, H.: PhD thesis: Micro-CT Imaging and Pore Network Extraction, Imperial College London, 2007.

41) Dullien, F. A. L.: Porous Media: Fluid Transport and Pore Structure, 2nd ed., Academic, San Diego, Calif, 1992.

42) Flett, M., Gurton, R. and Taggart, I.: The Function of Gas-Water Relative Permeability Hysteresis in the Sequestration of Carbon Dioxide in Saline Formations, SPE 88485, Proceedings of Asia Pacific Oil and Gas Conference and Exhibition, Perth, Australia, 18-20 October, 2004.

43) Mo, S. and Akervoll, I.: Modelling Long-term CO_2 Storage in Aquifer with a Black-Oil Reservoir Simulator, SPE 93951, Proceeding of the SPE/EPA/DOE Exploration and Production Environmental Conference, Galveston, Texas, 7-9 March, 2005.

44) King, M.B., Mubarak, A., Kim, J.D. and Bott, T.R.: The Mutual Solubilities of Water with Supercritical and Liquid Carbon Dioxide, Journal of Supercritical Fluids, 5, 296-302, 1992.

45) Pruess, K. and Spycher, N.: ECO2N - A Fluid Property Module for the TOUGH2 Code for Studies of CO_2 Storage in Saline Aquifers, Energy Conversion & Management, 48, 1761-1767, 2007.

46) Ennis-King, J. and Paterson, L.: Role of Convective Mixing in the Long-term Storage of Carbon Dioxide in Deep Saline Formation, SPE Journal, 10, 349-356, September, 2005.

47) Xu, T., Apps, J. A. and Pruess, K.: Reactive Geochemical Transport Simulation to Study Mineral Trapping for CO_2 Disposal in Deep Saline Arenaceous Aquifers, J. Geophys. Res., 108(B2), 2003.

48) Bruant, R. G., Jr., Celia, M. A., Guswa, A. J. and Peters, C. A.: Safe Storage of CO_2 in Deep Saline Aquifers, Environmental Science and Technology, 36(11), 240A-245A, 2002.

49) Juanes, R., Spiteri E. J., Orr, F. M. Jr., and Blunt M. J., 2006, Impact of relative permeability hysteresis on geological CO_2 storage, Water Resources Res., 42.

50) Jiang, X., 2011, A review of physical modelling and numerical simulation of long-term geological storage of CO_2. Applied Energy, 88(11), 3557–3566.

51) Rochelle, C.A., Czernichowski-Lauriol, I., Milodowski, A.E., 2004, The impact of chemical reactions in CO_2 storage in geologic formations: a brief review. In: Baines, S.J. and Worden, R.H (eds) Geological Storage of Carbon Dioxide, Geological Society, London, Special publications, 233: 87–106.

52) Gaus, I., Azaroual, M. and Czernichowski Lauriol, I., 2005, Reactive transport modelling of the impact of CO_2 injection on the clayey caprock at Sleipner (North Sea), Chemical Geology, 217(3-4): 319-337.

53) Cailly, B., Le Thiez, P., Egermann, P., Audibert, A., Vidal-Gilbert, S., Longaygue, X., 2005, Geological storage of CO_2: A state-of-the-art of injection processes and technologies, Oil and Gas Science and Technology - Review IFP, 60(3): 517-525.

54) André, L., Audigane, P., Azaroual, M. and Menjoz, A., 2007, Numerical modelling of fluid-rock chemical interactions at the supercritical CO_2 -liquid interface during CO_2 injection into a carbonate reservoir, the Dogger aquifer (Paris Basin, France), Energy Conversion and Management, 48(6): 1782.

55) Alkan, H., Cinar, Y. and Ulker, E., 2010, Impact of Capillary Pressure, Salinity and in situ Conditions on CO_2 Injection into Saline Aquifers, Transport in Porous Media, 84(3): 799-819.

56) Gündoğan Ö. Geochemical Modelling of CO_2 Storage. PhD Dissertation, Heriot-Watt University, Edinburgh, 2011.

57) Oelkers, E.H., Benezeth, P. and Pokrovski, G.S., 2009, Thermodynamic databases for water-rock interaction, Reviews in Mineralogy and Geochemistry, 70(1): 1-46.

58) Harvey, A.H., 1996, Semiempirical correlation for Henry's constants over large temperature ranges, AIChE Journal, 42(5): 1491-1494.

59) Soave, G., 1972, Equilibrium constants from a modified Redlich-Kwong Equation of State, Chemical Engineering Science, 27(6-A): 1197-1203.

60) Peng, D.Y. and Robinson, D.B., 1976, A new two-constant Equation of State, Industrial & Engineering Chemistry Fundamentals, 15(1): 59-64.

61) Li, Y.-K. and Nghiem, L.X., "Phase Equilibria of Oil, Gas and Water/Brine Mixtures from a Cubic Equation of State and Henry's Law", Can. J. Chem. Eng., (June 1986) pp. 486-496

62) Average annual atmospheric CO2 concentrations based on direct measurements at Mauna Loa Observatory from 1960–2009 (NOAA/ESRL).

63) Niessner J, Helmig R. Multi-scale modelling of two-phase–two-component processes in heterogeneous porous media. Numer Linear Algebra Appl 2006;13(9):699–715.

64) Ministry of Economy, Trade and Industry, Global Warming Countermeasure Technology Promotion Project (Examination of CCS Possibility in Onshore Oil Fields, Mexico) Report, Japan, 2016.

65) Xu T, Sonnenthal E, Spycher N, Pruess K. TOUGHREACT – a simulation program for non-isothermal multiphase reactive geochemical transport in variably saturated geologic media: applications to geothermal injectivity and CO2 geological sequestration. Computation Geosciences 2006;32(2):145–65.

66) Darcy H. Les Fontaines Publiques de La Ville de Dijon (The Public Fountains of the Town of Dijon), Dalmont, Paris, 1856.

67) Helmig R. Multiphase flow and transport processes in the subsurface - a contribution to the modelling of hydrosystems. Berlin: Springer; 1997.

68) Li H, Yan J, Yan J, Anheden M. Impurity impacts on the purification process inoxy-fuel combustion-based CO2 capture and storage system. Appl Energy 2009;86(2):202–13.

69) Juanes R. Displacement theory and multiscale numerical modelling of three-phase flow in porous media. PhD Dissertation, University of California, Berkeley, CA; 2003.

70) Nikolova K., Angelov A., Bratkova S., Plochev S., Implementation of EU requirements on carbon capture and storage in Bulgarian environmental legislation, Sofia, 2012.

71) Class H, Ebigbo A, Helmig R, Dahle HK, Nordbotten JM, Celia MA, et al. A benchmark study on problems related to CO2 storage in geologic formations. Computational Geosciences 2009;13(4):409–34.

72) Brooks, R.H. and Corey, A.T. 1964. Hydraulic Properties of Porous Media. Hydrology Papers, No. 3, Colorado State U., Fort Collins, Colorado.

73) Pamukcu Y., Hurter S., Jammes L., Dat Vu-Hoang, and Pekot L. Characterizing and predicting short term performance for the in Salah Krechba field CCS joint industry project. 10th International Conference on Greenhouse Gas Control

Technologies, Amsterdam, Netherlands, 19 - 23 September 2010. Amsterdam, Netherlands.

74) Land, C. S.: Calculation of Imbibition Relative Permeability for Two and Three-Phase Flow from Rock Properties, SPE Journal, 149-156, June, 1968.

75) Li, Y.-K. and Nghiem, L.X., "Phase Equilibria of Oil, Gas and Water/Brine Mixtures from a Cubic Equation of State and Henry's Law", Can. J. Chem. Eng., (June 1986) pp. 486-496.

76) Helgeson, H.C., 1969, Thermodynamics of hydrothermal systems at elevated temperatures and pressures, Am J Sci, 267: 729-804.

LIST OF FIGURES

Figure 49: 8_Case: CO_2 trapped, dissolved, mineral, and aqueous ions.

LIST OF TABLES